Experimental Setup and Testing of Fiber Reinforced Composite Structures

by

Scott Robert John Bumpus
Bachelor of Engineering, University of Victoria, 2002

A Thesis Submitted in Partial Fulfillment of the
Requirements for the Degree of
MASTER OF APPLIED SCIENCE
in the
Department of Mechanical Engineering.

University of Victoria

Supervisors: Dr. Afzal Suleman

Abstract

Fiber-reinforced composite structures have seen an increased application in aeronautics and in other industries such as automotive, marine transportation, civil engineering, sporting goods, medical equipment and prosthetic devices. With the increased use of composite materials, there is a need to develop methods to predict the material properties and behavior of composite materials and structures made of these materials under a variety of loading and environmental conditions.

In this thesis, an experimental test procedure was designed and implemented to determine the mechanical properties of fiber reinforced composite structures. Resin transfer molding was used to manufacture the test specimens. Large panels were molded with different constituent concentrations. The test coupons were cut from a single plate using a water-jet cutting technique. Tensile and flexural tests were performed and tables of new material properties have been created. Each of the specimens were tested in a random order and the stress and strain data was calculated from the load and displacement results. The experimental tests were performed at two perpendicular orientations to determine the influence of fiber orientation on the material mechanical properties. Experimental values were obtained for tensile modulus, maximum stress, the strain at maximum stress, and Poissons ratio in all three directions.

Table of Contents

List of Tables

List of Figures

Acknowledgements

I would like to thank my supervisor, Dr. Afzal Suleman, for his support and guidance throughout the time it took to complete this thesis and my degree. The graduate research assistance provided by ASI BC and Profile Composites Inc. is acknowledged. I would also really like to thank the people at Profile Composites Inc; Geoff Wood, Peter, Quinn, Graham, Ryan, Tamra, and Dan. Thanks to Sean Taylor at Aquashear for dealing with all the panels cut and the specific requirements that came with that task. I would also like to thank my graduate student colleagues working under Dr. Suleman, Sandra Makosinski, and the mechanical engineering graduate secretaries for their support, suggestions, and friendship throughout this degree. Last but not least I would like to thank my friends and family for their support.

Chapter 1

Introduction

Historically a predominantly aerospace material, fiber-reinforced composite structures have seen an increased application in other industries such as automotive, marine transportation, civil engineering, sporting goods, medical equipment and prosthetic devices. Fiber-reinforced composite structures provide high strength, high stiffness mechanical properties, unique flexibility in design capabilities, and ease of fabrication. Also, they are lightweight, corrosion resistant, impact resistant, and have excellent fatigue strength. With the increased use of composite materials, there is a need to develop methods to predict the material properties and behavior of composite materials and structures under a variety of loading and environmental conditions.

Fiber-reinforced composites are composed of two or more materials which, when properly combined, form a different material with properties not available from the ingredients alone. Depending on the ingredients chosen and the method of combining them, a large spectrum of material properties can be achieved. A brittle material can be made more ductile (flexible) by adding a softer material; conversely a soft material can be made stiffer. Wood is a good example of a composite. The cellulose fibers provide the strength and are held together by the resin. Reinforced concrete is

another example. The steel re-bars provide excellent tensile strength and the concrete provides compressive strength and transfers the load between the steel bars. Modern composites or FRP (Fiber reinforced polymers, or plastics) are the newest addition to the structural engineers toolbox. Although the materials have been available for decades, a reduction in cost, combined with newer understanding of the versatility and benefits of the material properties, has allowed composites to move into mainstream construction.

Composite properties are phase dependent, and every phase included in the composite has a significant effect on overall material properties. There are a number of models that can be used to predict the composite properties, but the more accurate the model, the more one must know about the different phases. Extensive tests must be carried out on the individual phases to determine the material properties that are used for a specific model. Even if the properties of the materials are known, these are considered an approximation due to the intrinsic nature of composites. To demonstrate this point, the composites factor of safety in the marine industry is taken as 10 [1].

1.1 Background and Motivation

There are a number of methods for manufacturing composite structures. The predominant method used in the aerospace and other high cost industries is the autoclave method. Another common method of composites construction is resin transfer molding (RTM). This more modern method is a faster and more cost effective way to create parts. Comparisons of these methods have been reported in the literature such as [2, 3]. The autoclave has been around for a longer period and is therefore a more researched and well known method. However, the RTM method is becoming more

wide spread and further research is being conducted due its lower cost production. The cost savings comes from faster production and lower material costs.

For the autoclave production method, the part is first molded using a prepreg material. A prepreg consists of fibers in sheet form already impregnated with resin. The prepreg is placed in a mold and then heated to 120-180°C and at this temperature the resin cures. The part is placed in the autoclave which is a large temperature pressure vessel. The temperature is then raised and the pressure is increased in order to consolidate the part, thus removing air bubbles and squeezing out any extra resin. Bringing the autoclave up to temperature is a slow process which depends largely on the size of the autoclave. The pressure chamber can reach up to 5 bars, creating very high quality and consistent parts.

Resin transfer molding is a process which involves placing dry fibers in a mold and adding the resin separately. Resin is injected in the mold at the inlet port (or ports depending on how the mold is designed) until it flows out the outlets and the fibers become completely wetted out. The mold can be a closed mold or it can be composed of a single flow surface and a vacuum bag. A vacuum bag is just a thin film that covers the fiber preform and is connected to the base of the mold, or it may encompass the entire mold. A vacuum is then pulled on the part in order to impart a one atmosphere pressure over the part surface. This process provides for a large reduction in cost because purchasing the fibers and resin separately are cheaper than prepreg materials, and vacuum bags are much cheaper than an autoclave. Also, cure times are faster because a catalyst is used in RTM as an alternative to waiting for the system to get to really high temperatures. As an example, Ramulu et al. [4] reported cure times of 27 to 32 hours to create panels using the autoclave method. During the course of this thesis, it was possible to manufacture 5 panels in a single day using the RTM procedure.

The advantage of using an autoclave over an RTM process is that it produces higher fiber concentrations. Due to the higher pressures involved, it packs the fibers tighter and essentially squeezes the resin into small areas between fibers that may not be possible using the RTM process. McIlhagger et al. [3] did a comparison with similar input fiber and resin and found about a 25.7-27.2% reduction in flexural properties and a 15-17.7% reduction in tensile properties. When using the RTM method, Marsh [5], also concluded that RTM is a technology that can produce a part in minutes which would take hours or even days with previous technology. This is one of the reasons that autoclaves are still used in the aerospace industry, however for parts that do not require such high quality, the RTM can be a very affordable solution. For example, in the automotive industry there are numerous parts that do not require such high quality composites.

Hybrid composites have been extensively studied and reported in the open literature. Continuous fiber oriented hybrid composites have been studied by Junior et al. [6] and are a very popular composite because of its superior strength characteristics. Also, Fu et al. [7, 8] have done extensive research on short fiber composites. These short fibers are on average less than 1mm in length and are mixed with the resin matrix prior to being injection molded to create the samples. Joseph et al. [9] and Rana et al. [10] also investigated this composite with a maximum unbroken fiber length of about 10mm. This method is simple but results in weak reinforcement due to the short fiber lengths.

The main purpose of this thesis is to create a database of tensile and flexural properties for chopped fiber composite structures. With this information, models can be created to predict how different phase combinations effect the composite material properties. A large number of tests were performed. Also in order to ensure that the data is statistically accurate, a number of replicate tests were performed and a

statistic method based on the Design of Experiments (DOE) was used.

Design of Experiments (DOE) is a method for selecting the best combinations of factors in order to determine the optimal response of the system. Given a test matrix, the DOE determines the necessary experiments and the appropriate order of testing. The method is used to reduce the number of experiments by testing the extremes of the test matrix and determining the factors that do not significantly affect the response of the experiment.

Sutherland [1] has done a number of tests using design of experiments and has found large deviations in the results when testing composites. He has concluded that when designing an experiment to test a composite material, it is difficult to perform fractional factorial designs. Fractional factorial designs allow the experimenter to further reduce the number of tests. It is a technique used when there are a large number of input variables. It allows the researcher to find out information on all the factors without actually running every combination of variables.

1.2 Testing Guidelines

In the current research, two fiber phases are examined: the carbon fiber (TORAY T700SC -12000 -50C) and the E-glass fiber (from either PPG or Owens Corning®). Polymat "Hi Flow" made by "Scott and Fyfe" is used as a core for the composites. This core is a prefabricated material that contains a polypropylene core with random chopped E-glass mat stitched to both surfaces. The resin phase is a urethane and polyester hybrid resin system (DION ITP 31638-00). A preform is created from the Hi Flow core with extra glass or carbon chopped fibers added as needed to both sides of the core. The method for making the composite used in this research is resin transfer molding (RTM). Test samples were manufactured from a series of composite

sheets about 30cm x 60cm and the test coupons were cut out of the sheet using a waterjet cutter.

ASTM D3039 [11] is used for determining tensile properties. The shape of the tensile coupon is taken from ASTM D368 [12]. ASTM D790 [13] is used as the guideline for performing the flexure tests. These are the recommended ASTM test procedures by the Mil Handbook 17 [14] and have been used by other researchers such as [4, 15].

With plastics in general, tensile and flexural properties are tested independently. The tests determine the elastic modulus, the maximum stress, and the strain at maximum stress for the material in tension and flexure, as plastics behave differently in these two modes. ASTM D790 has been adapted from a strictly plastics test and is not reliable for determining actual flexural properties of composites. The Mil Handbook 17 does not recommend using the flexural properties. In the aerospace industry, flexure testing is used mainly for quality control [14]. These tests have been reported in the literature by [10, 16], and are used to compare production methods and composite compositions.

The experiments were performed on an MTS hydraulic test machine. The machine has a load cell to measure the applied force. For tensile tests, an MTS biaxial extensometer is used for calculating the strain in the axial direction, in either the width or the thickness direction of the specimen. This allows the Poisson's ratio to be calculated. The flexure tests are performed using a three-point bending jig and the displacement is measured using the sensor on the MTS machine.

1.3 Scope of the Thesis

The motivation for this thesis is to test hybrid composites that can be used for replacing traditional construction materials in automobiles and similar applications. Advanced composites can have better strength to weight characteristics than traditional materials such as steel and aluminum. There is also the potential for cost reduction.

In this thesis, a table of properties for the destructive tensile and bending tests was constructed. The factors to be considered are shown in Table 1.1. Factors like temperature have not been considered.

Factor	Value Range
Carbon Percentage	0% - 57%
Specimen Thickness	3mm - 6mm
Fiber Angle	Random orientation

Table 1.1: Factor Ranges

The results of the tests have been analyzed using the statistical design of experiments tools. This technique provides the amount each factor contributes to the strength of the material and the interaction effects between factors.

1.4 Structure of the Thesis

The thesis is composed of 5 chapters. Chapter 1 presents the background and motivation of the thesis. Chapter 2 presents the experimental setup and the fabrication of the test coupons. Several techniques were attempted to create the test coupons, and this chapter describes the steps taken to manufacture the test specimens. Chapter 3 discusses the analysis of the raw data and how the design of experiments method is

used to help perform the experiments in a reliable and systematic manner. Chapter 4 states the results and findings of the experiments. The results are then compared to numerical data obtained using a basic rule of mixtures model and a response surface model. Finally, the conclusions and future work is outlined in Chapter 5.

Chapter 2

Testing Environment Design and Setup

In this chapter, the design and manufacturing process for the test coupons are described. The manufacturing process was carried out at Profile Composites Inc. The dimensions of the test coupons and method of testing used in this research were determined using the American Society for Testing and Materials (ASTM) standards.

The tensile coupons were designed in accordance with ASTM standard D 638 - 99 [12]. According to the standard, the specimen should be a "dogbone" shape. If the material is less than 7mm thick the width should be 13±0.5mm with a length of the narrow straight section of 57±0.5mm. ASTM standard D3039 [11] is the standard for polymer matrix composites. The dogbone shape was chosen to ensure that the samples would break in the gauge area. D3039 cautions that samples should be individually molded or if cut from a panel care must be taken to avoid a rough finish from the cut or delamination as a result of poor cutting methods.

The flexure coupons were designed based on ASTM standard D790 [13]. The

specifications for the size of the coupons given in the standard are that the specimen width shall not exceed 1/4 the support span. The support span is 16±1 times the specimen thickness. The ends of the specimen should extend at least 10% of the support span over the support. The dimensions chosen to fulfill these requirements were 13mm wide by 126mm long.

2.1 Coupon Manufacturing Methods

Resin Transfer Molding is a common composite manufacturing process. The pre-catalysed resin is injected into a mold containing the dry reinforcing material arranged in the desired number of plies and orientation. The injection pressure varies between 0.5-4 bars while the curing of the resin is often assisted by heating.

2.1.1 Small Scale Resin Transfer Molding

In the first instance, it was decided that the composite coupons would be molded individually using a small scale resin transfer molding process. One mold was made for two tensile test coupons and another mold was made for two flexure test coupons (see Figure 2.1).

These molds were made from 1.25 inches thick aluminum on the bottom and 1 inch thick on the top. These dimensions were determined so that the mold can be at least 1 inch larger than the part in all directions. This allowed for high temperature injection molding of plastics so that the molds could be used for testing plastics properties as well. They were created for use on a 20 ton Morgan injection molder. The molds were also created with the intention to use them for resin transfer molding and thus have injection ports on the edge of the molds as well. The two injection

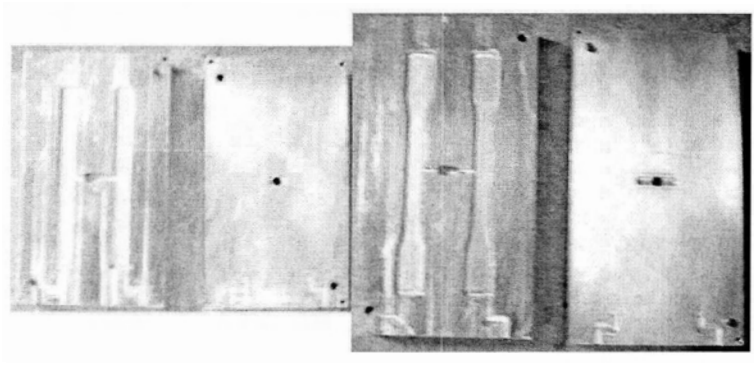

Figure 2.1: Small Scale Molds: Flexure Mold (left) and Tensile Mold (right)

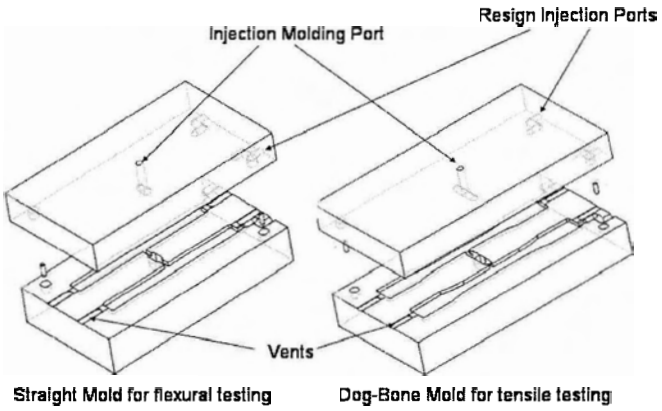

Figure 2.2: Injection Port Options: Flexure Mold (left) and Tensile Mold (right)

port choices are illustrated in Figure 2.2.

In order for the molds to be designed properly there are a number of features that must be included [17]. All cuts into the mold must be tapered by at least 2^o. That includes the edges of the test coupons and the central injection port on both molds. Under the central injection port there is a small cavity to capture the initial shot of

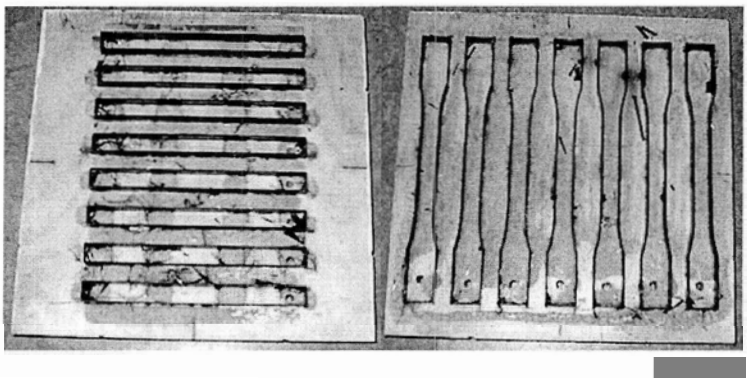

Figure 2.3: Steel Rule Dies: Flexure (left) and Tensile (right)

injected plastic because it has a tendency to not be fully melted and would not allow proper flow of the plastic. In order to get the injected material to all parts of the mold without air bubbles, the mold must be properly vented. These vents are only 0.5mm deep to allow the overflow to be cleanly trimmed from the finish part. The gates where the injection ports meet the specimen cavity must be designed properly so they are not too large, making it difficult to remove from the finished product, or too small, making it impossible to get the necessary flow rates in order to get the injected plastic to the ends of the cavity before it solidifies. The chosen size was to have the gate as wide as the depth of the cavity.

Before coupon production could commence tools had to be created to cut the fibers into the shape of the mold cavities, steel rule dies were chosen for this task. These are essentially like a cookie cutter and are illustrated in Figure 2.3. They consist of steel bands with a knife edge on one side which are inserted into a plywood backing in the desired shape of the object to be cut. The fibers are sprayed into a flat mat preform and then a 20 ton press is used to stamp the shapes of the steel rule dies out of the mat. These preforms are then inserted into the molds to create the coupons.

The process of creating the coupons is to first create a preform mat so that the coupon shapes can be cut out. These mats were constructed using E-glass mat stitched to a Rovacore center as the base. This mat was used before the "Hi Flow" mat was found to be better. 3M contact cement is then sprayed on the E-glass mat as a binder for the carbon fibers. Carbon fibers are then sprayed onto both sides of the mat from the chopper gun to the desired thickness of fibers. This preform is then stamped to the specimen shape using the steel rule die. The mold is preheated in the oven. It is then removed from the oven and a mold release is sprayed into the mold cavity for easy sample removal when curing has occurred. The fiber preform is then placed in the mold and the appropriate plugs are placed in the injection ports that are not to be used. The top half of the mold is connected to the bottom and four hand screw clamps are used, one on each corner of the mold for a good seal (see Figure 2.4). The mold with the clamps in place is then inserted in the oven to bring it back to a good molding temperature. Once the mold is up to temperature the resin is mixed and the mold is once again removed from the oven and the resin is injected into the mold port using a syringe with sealing tape around the nozzle. After the injection is complete the excess resin is wiped off the mold. After the specimens have cured they are removed and the mold is scraped clean of excess resin and prepared for the next samples.

This molding technique had a few problems that made it an unfeasible method for coupon production. The molds were very ridged in their design making it very difficult to vary specimen thickness. Inserts would have to be used to decrease specimen thickness and spacers would have to be used to make the specimen thicker. Inserts would be difficult to remove after the resin cures. Also, the steel rule dies were very difficult to use. The dies were very sensitive to the slightest variations in the steel height. The carbon fibers used have a filament diameter of 7μm, making it exceedingly

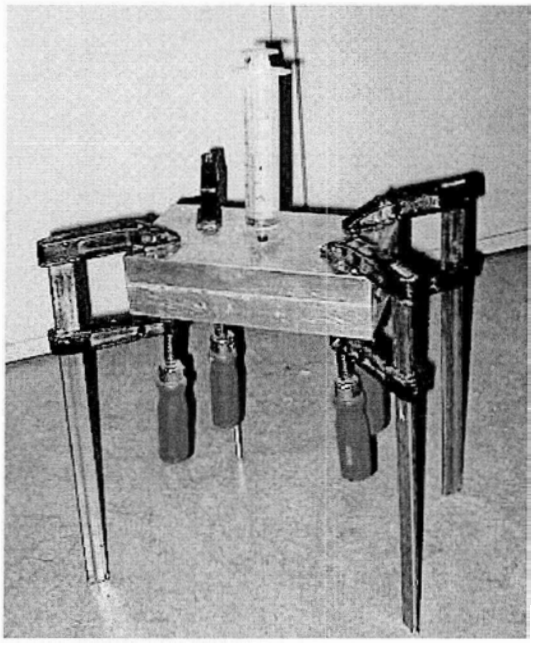

Figure 2.4: Mold Ready For Injection

difficult to make a perfectly clean cut. When a group of filaments is left uncut, upon removing the stamped shape it may still be connected to the source material creating a shift in the fibers before the filaments break away from the shape or the attached filaments cause a large section of fibers to be removed from the stamped shape. Also when removing the preform from the dies, the preform would often come apart and would not maintain its original shape.

In order to ensure the fiber preform would fit easily in the mold the steel rule dies were created slightly smaller than the mold. This created a problem. When the resin was injected it would push the fiber to one side of the mold and there would be a strip of un-reinforced resin as seen in Figure 2.5. This results in a need to machine out the un-reinforced resin because the inconsistency would give inaccurate results. The machining of the specimens would be counter productive to the molding process.

The problem is further complicated by the fact that sometimes the fiber would not be pushed all the way to one side so the un-reinforced resin would have to be removed from both sides of the specimen. The objective of molding individual samples was to test the samples straight out of the mold, but the need to machine the samples would create an unnecessary overhead to the process.

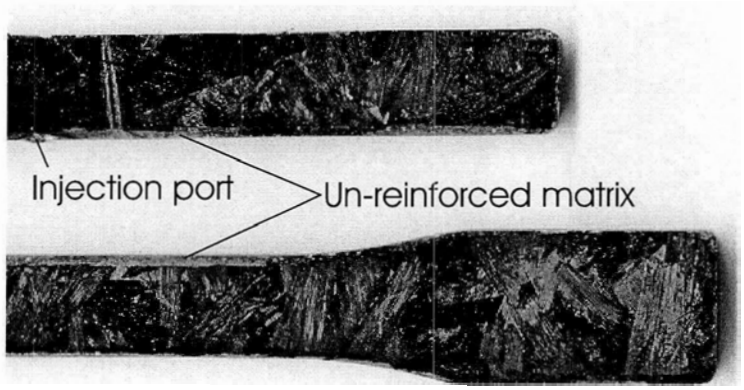

Figure 2.5: Molded Test Coupons: Flexure (top) and Tensile (Bottom)

These factors made the small scale injection molding impractical. It was decided to manufacture a large panel and cut the individual coupon samples from this panel. This process is discussed in the next section.

2.1.2 Large Scale Injection Molding

The method used to create the test coupons was to use a resin transfer process similar to the individual sample creation process described above. The fundamental difference is that instead of molding just two coupons at once, a panel about 30cm by 60cm was created and the coupons were cut from the panel. This is accomplished using the mold shown in Figure 2.6.

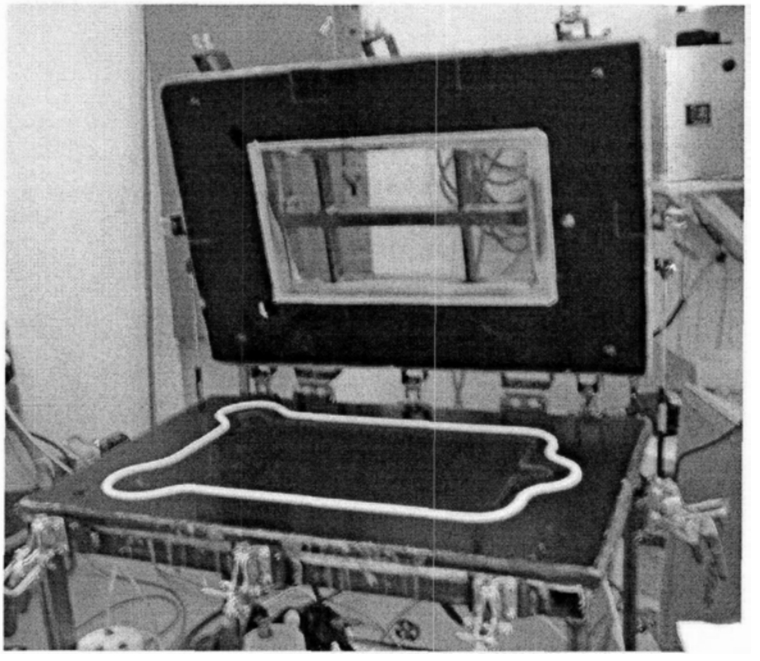

Figure 2.6: Mold for Creating Large Flat Composite Panels

The mold consists of a steel frame with eight locking clamps around the edge. The mold surface is created from a composite that is formed in the shape of the mold and is coated with a smooth gel coat surface. Embedded in the bottom of the composite mold is a system of pipes as seen in Figure 2.7. Hot water is pumped into this piping and is used to heat the mold. This allows for the mold to be brought up to the optimum cure temperature of the resin matrix which is 45°C. In the top of the mold is a glass window which allows the operator to view the resin flow front as the part is injected. At one end of the mold is the inlet port for the resin to be injected. At the other end are two exit holes to allow the resin to flow through the fiber preform and escape. The exit holes are connected to a cylinder from which a vacuum is pulled to enhance flow and collect excess resin.

After the preform is created the mold is preheated to about 45°C. The preform is

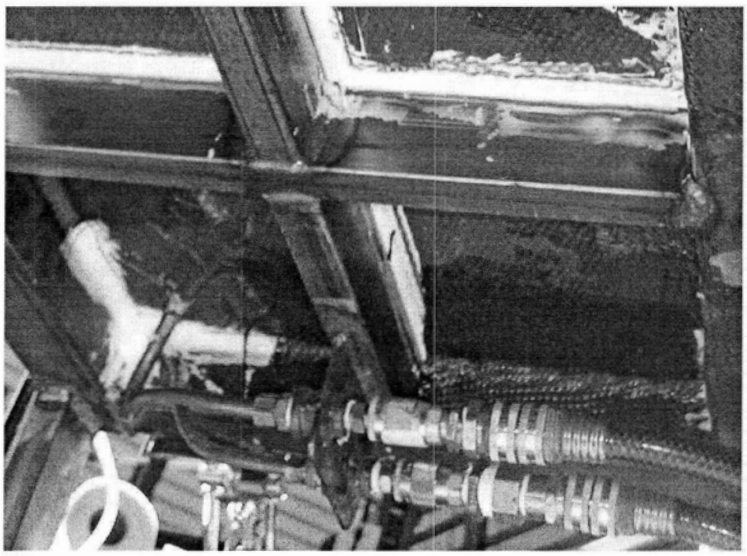

Figure 2.7: Inlet and Outlet for Mold Heating System

then placed in the mold and an inflatable o-ring type dynamic seal is placed around the mold cavity so that the resin is stopped from escaping though the sides of the mold. Two rubber strips are then laid between the seal and the preform to block the resin from traveling down the sides of the preform instead of through the preform. After the seal is in place and the mold is closed up and clamped, the seal is then inflated to between 20 and 50 psi depending on desired thickness of the part. The resin used is a three part hybrid resin system. It consists of a polyester resin, a polyurethane resin, and a catalyst. The resin is mixed to the desired ratios and pumped using the equipment seen in Figure 2.8. This equipment also keeps the resin heated to about 45°C. The resin is pumped into a pressure pot and initially the resin is injected by pulling a vacuum in the mold. After the part is completely wetted out and resin flows out the outlet ports, or 5.5 minutes after the injection started, the vacuum is removed and the pressure pot is used to provide positive pressure. At about 7 minutes after the start of injection the outlet lines are pinched off and the

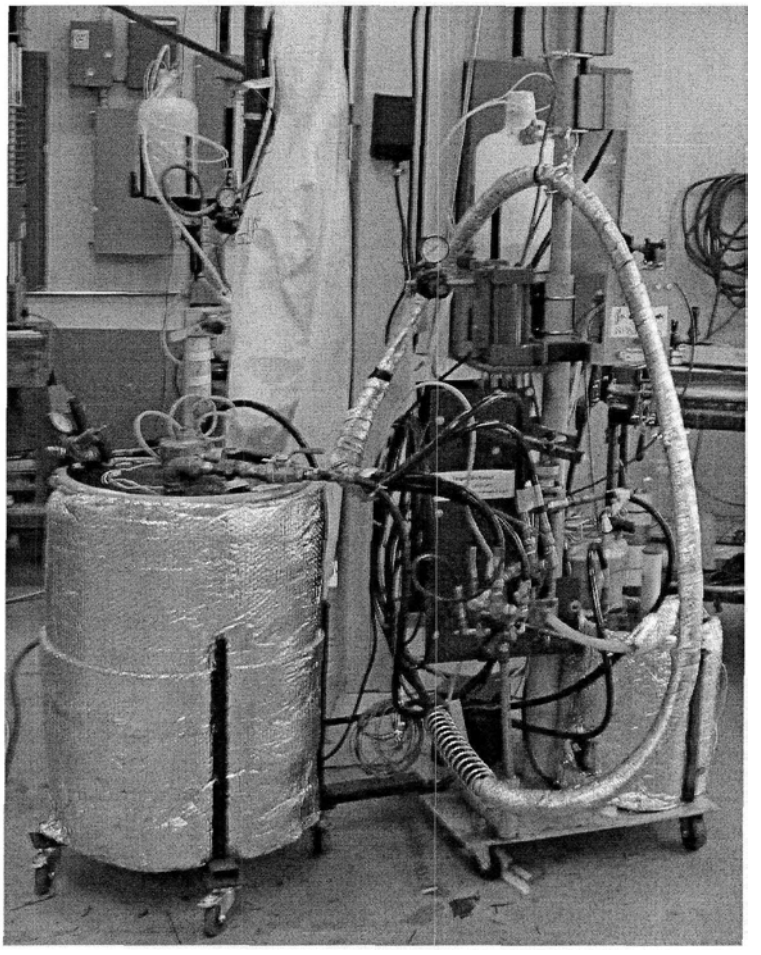

Figure 2.8: Resin Mixer and Pump For Hybrid Resin

resin is pumped in for about 45 seconds more. The timing is critical because the resin starts to cure about 8 minutes after it is mixed. A picture of the resin flow front from the window in the top of the mold can be seen in Figure 2.9.

After the resin has cured the mold can be opened and the completed composite removed. The composite panel is then shipped to Aquashear in Vancouver so the test coupon shapes can be cut using a high pressure water jet with the equipment seen

Figure 2.9: Resin Flow Pattern Through the Composite

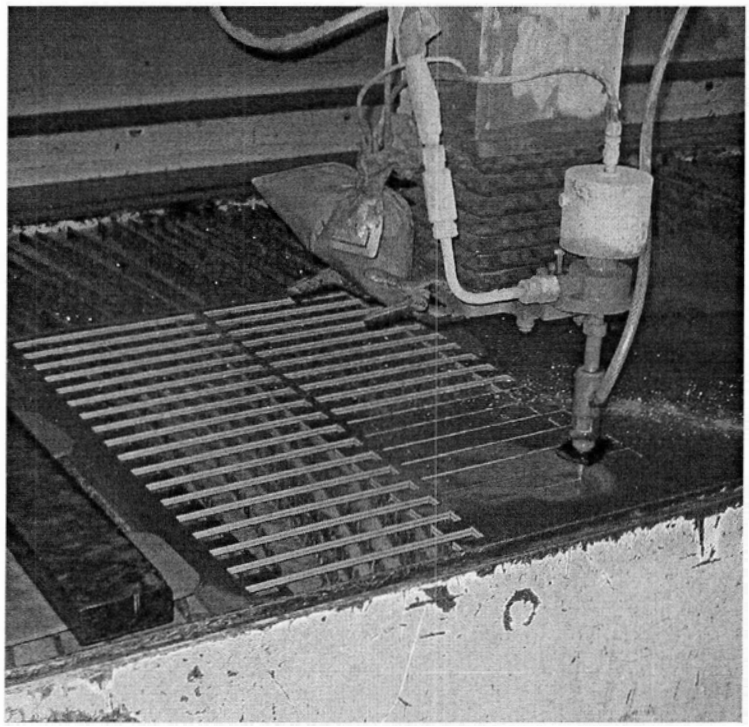

Figure 2.10: Water Jet Cutter

in Figure 2.10. This water-jet cutting is very useful for composites because to cut them with a saw requires diamond tipped cutters and produces dust that is harmful to breathe. The water-jet cutter can start a cut in the middle of the sheet, it is computer controlled, and the cut is only 0.8mm wide. The piece to cut is placed on sacrificial steel strips which are suspended above a large tank of water. The high pressure water cuts the material and then defuses into the water tank below.

Manufacturing Issues

The large mold method is not free of problems. One problem is that the thickness throughout the panel is not uniform. This is due to flexing in the mold during the

injection and curing process. This results in up to a 20% increase in thickness from the edge of the panel to the center.

Originally the resin was injected into the preform only by drawing a vacuum. This caused a significant amount of air bubbles in the panel. By curing a cup of resin in a vacuum chamber it was discovered that the vacuum was causing small bubbles to form in the resin. The process was changed to start with drawing a vacuum and then turning off the vacuum and applying positive pressure to 'push' the resin in instead of 'pulling' it with the vacuum, thus minimizing the bubbles.

The preform design proved to be a difficult process. Initially the same process was used as the small scale RTM method. A rectangular section of the Rovacore mat was cut to the dimensions of the mold cavity. 3M contact cement was applied to each side and carbon is added by visual inspection to both sides equally. This was not a very accurate way of adding carbon. When these preforms were used in the mold problems developed stemming from inability of resin to flow through the preform. The problem that would occur was that the preform was not fully wetted so there would be dry fiber in the final part. Also, for thin panels the fiber would be packed especially close together and the resin, when injected, would push the preform down the mold cavity and the part would be unusable. The preform process developed into more careful addition of fibers, a different core, and a different binding agent.

The final method of preform creation is as follows. A container was created the size of the mold cavity, this can be seen in Figure 2.11. This container is placed on a scale and the scale is zeroed. The core mat is placed in the container and weighed. Binder is sprayed on the exposed surface of the mat and the scale is zeroed again. If glass fiber is to be added, it is added at this stage. The glass fibers are chopped into a bucket and sprinkled on by hand because the chopper gun cannot chop the glass fibers as easily as the carbon fibers. The chopper gun produces fibers that are

about 30mm in length. After the glass is added, more binder is sprayed and the scale is zeroed again. The carbon fiber is then sprayed on using the chopper gun. The preform is then flipped over and the process is repeated on the other side. With the scale under the container it is easy to determine how much fiber is being added. Care must be taken to ensure even distribution of fibers and make sure there are no bare spots. It is very difficult to ensure even distribution and this is a likely cause for scatter in material data.

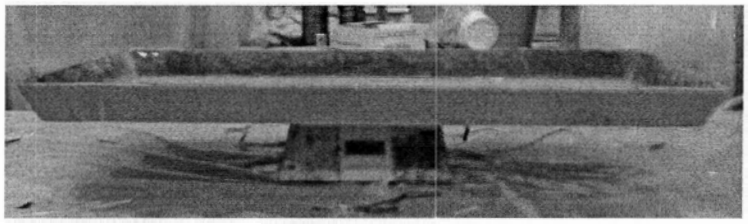

Figure 2.11: Preform Container On Scale

The core mat used is made by Scott and Fyfe and is called Polymat "Hi flow". The Polymat consists of two layers of glass chopped strand mat stich-bonded to a polypropylene core. The core allows the resin to flow through the middle of the glass sandwich and then the resin seeps out the the top and bottom surface. The Rovacore mat is supposed to behave similarly but the Polymat core allows the resin to flow much more freely, thus allowing the mold to be filled more smoothly. The binder used is called InfuZene. It is a spacial binder designed for use with polyester resin so that it does not inhibit curing, but actually redissolves into the resin during molding and helps the bond.

2.2 Cutting Pattern

Once the panels are cured they are removed from the mold and the edges are trimmed using a circular tile saw with a diamond blade. The panel is then weighed and measured so that the percentage of carbon fibers, E-glass fibers, and resin can be determined. This calculation is made assuming no loss of fiber weight after the trimming has occurred. The pattern used for samples to be cut from the panel can be seen in Figure 2.12. The ASTM standards state that at least five samples per composite should be tested. Six was the chosen number of samples because this would allow for three measurements of Poisson's ratio in each direction (thickness and width directions). This pattern was chosen because it allows six samples in the vertical direction and horizontal direction. There are actually nine samples cut horizontally, this is because there is enough space on the panel so if a sample must be discarded for some reason there are others to replace it. The problem with this layout is that all the vertical samples are down the sides of the panel and all the horizontal samples are down the middle. This is not a good layout because if the properties in the middle are different to the properties at the edge it may be confused with an orientation effect.

The pattern is printed out on paper and the sample shapes are cut out of the paper to leave a master template. This template is placed over the panel and each sample is numbered with a silver paint marker. Consistent numbering of the samples allows comparison of results with the knowledge of where it was cut from on the panel. With this information position influences can potentially be investigated. The Autocad file of the pattern is sent to Aquashear along with the panels. They line up the cutter in the same position as the template was lined up and the samples are cut and shipped ready for testing.

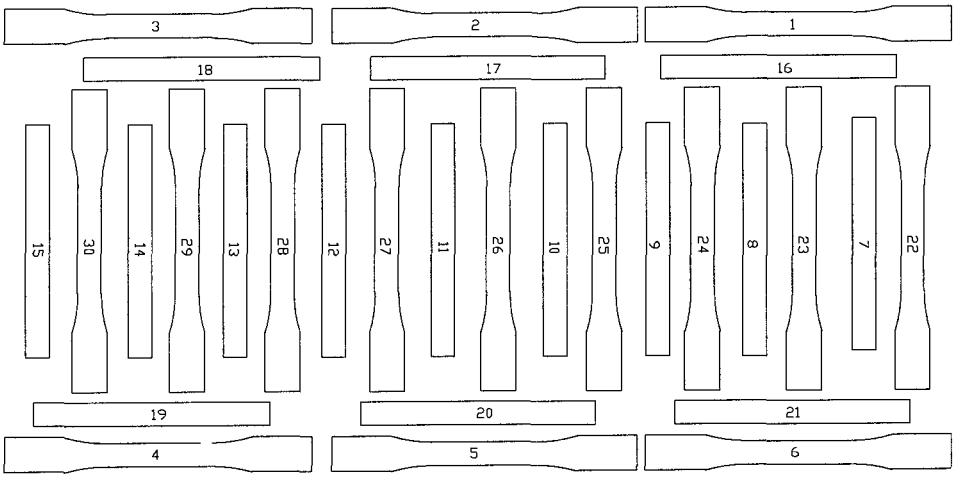

Figure 2.12: Water Jet Cutting Pattern for Panels

2.3 Test Procedures

In both types of tests the specimen must first be measured. The critical measurements are the thickness and width of the specimen. The dimensions are important in order to get accurate results due to the fact that some of the material properties rely on the cross-sectional area. Before each specimen is tested the width and thickness are recorded in a text file named either tensile or flexure with the date the experiment is occurring. Also any abnormal feature noticed in the part is recorded.

2.3.1 Tensile

For the tensile tests, due to the smooth surface finish on the specimens, the metal grips for the MTS machine sometimes slip when tension is applied. To solve this problem, emery cloth is placed in the grips which provides enough friction to stop the slipping. Initially, before a specimen in loaded in the MTS machine the load cell channel is zeroed because it has a tendency to drift. The MTS machine is set

to a home position that is a good distance for specimen testing. A test specimen is carefully measured and the width and thickness of the neck region are recorded in a file along with the specimen and panel number and any observations made during the experiment run. The specimen is then placed in the grips, care is taken to ensure good alignment of the specimen. The biaxial extensometer is then placed on the specimen using the conical point grips. The conical points are placed in the center of the specimen, either on the edge or on the face depending on the data to be obtained. Alignment pins are used to ensure the axial extension gauge length will be exactly one inch. A picture of a specimen to be tested is shown in Figure 2.13. The transverse extension gauge length is either the initial material thickness or width depending on which is being monitored. The transverse channel must be zeroed using the signal conditioning software. Since the alignment pins are used for the axial direction the axial channel is automatically zeroed. The tensile setup for the TestStar IIs software is then run and the grips separate at a displacement rate of 12.7 mm/min. After complete fracture of the sample the test is stopped and no more data is collected. The specimen is then removed and kept for observation purposes.

2.3.2 Flexure

For flexure tests, the metal grips on the MTS machine are replaced by a three point bend test jig. According to the ASTM standard, the bottom supports of the three point bend test jig must be spaced apart 16±1 times the thickness of the specimen. Each of the pedestals must be set equally from the center of the jig so the load is applied at the center of the supports. Care must be taken to ensure that each of the cylindrical loading noses are aligned. The specimen is measured and the thickness and width are recorded in a file with the specimen and panel number. The support span is recorded in this file and any observations of the experiment are recorded as well. The

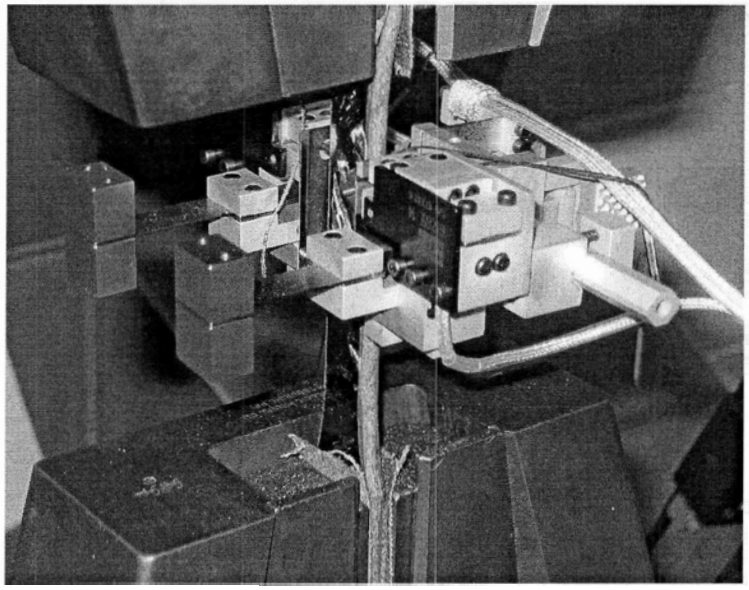

Figure 2.13: Specimen Loaded and Ready for Tensile Test

specimen is centered on the bottom pedestals and the top pedestal is hydraulically lowered to just above the surface of the specimen. A picture of a specimen ready to be tested is shown in Figure 2.14. The flexure setup for the TestStar IIs software is then run and the center loading nose is lowered at a rate of 15.2 mm/min. The program is stopped after significant breakage in the specimen occurs. The loading nose is then raised and the specimen is then removed and replaced by the next test.

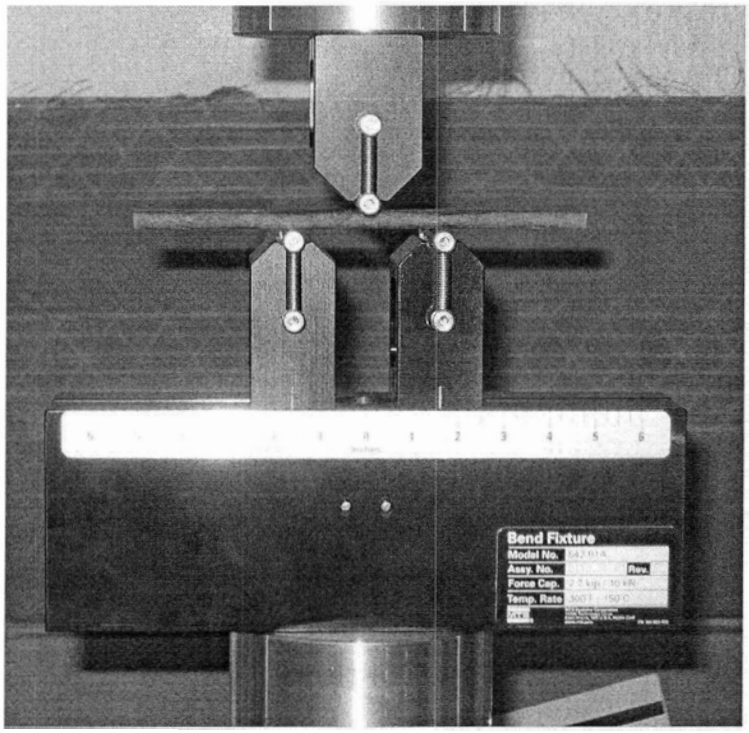

Figure 2.14: Specimen Loaded and Ready for Flexure Test

2.4 Synopsis

This chapter covers the selection of the size and shape for advanced composite test coupons using ASTM standards for tensile and flexure testing. In order to create these composite samples two separate resin transfer molding procedures were tested. The first involved molding each sample individually with the use of a small aluminum mold. The mold cavity consisted of two locations for the coupons to be molded to their final desired shape. The second method of coupon production involved using a larger steel mold to manufacture a large panel out of which test coupons were cut. The second method proved to be superior due to more efficient test coupon production. The tensile and flexure test procedures were outlined at the end of this chapter. The next chapter will discuss how the collected data was analyzed.

Chapter 3

Data Processing and Analysis

This chapter describes the analysis and processing of the large amount of data collected during the research. For tensile tests, the collected data includes the elapsed time, load, axial extension, transverse extension, and grip displacement. The load and extension data are critical in the analysis whereas the time and displacement data are collected in case they can be used in the future. For flexure tests the monitored variables are elapsed time, load, and load-nose displacement. Again load and displacement are critical for analysis and time data is just collected for completeness.

For both flexure and tensile tests, a Matlab script reads in the data file with the specimen number and specimen sizes and stores this data into an array. The script then reads in the necessary data columns from the file and stores the information in cell structured arrays. Each experiment is then scanned for the maximum load data point, this is recorded in an array and another subset of arrays is created with just the data prior to the peak load point. The relevant data can then be calculated and the results are discussed in the Tensile Data3.1.1 and Flexure Data3.1.2 sections. After the calculation of data, the results for each panel are inserted into the Microsoft Access database for convenient storage and further analysis.

3.1 Data Processing

3.1.1 Tensile Data

The properties that must be calculated in the tensile data scripts are Youngs modulus, maximum tensile strength and Poissons ratio in all directions. Initially, arrays of stress are created for each test by dividing the applied load by the specimens cross-sectional area, and arrays of strain by dividing the extensometer displacements by the initial gauge lengths. The maximum tensile stress data in this thesis is taken as the maximum from the stress array. Typically Youngs modulus would be found by plotting a stress verses strain curve and reading the slope of the initial linear portion of the curve. To simulate this the script takes the stress and strain data and fits a first order polynomial to the linear portion and the slope that is calculated is Youngs modulus for that test. The Poissons ratios are calculated in a similar manner except they use the strain data in two directions to calculate the relationship as in equation 3.1. It can also be seen in equation 3.1 that Poisson's ratio in one direction can be determined from the ratio in the two other directions. In this research the 23 direction is found from the 12 and 13 directions. The directions are defined in Figure 3.1.

$$\begin{aligned} \nu_{ij} = -\frac{\varepsilon_j}{\varepsilon_i} \, where : i \neq j \\ also : \\ \nu_{ij} = -\frac{\nu_{kj}}{\nu_{ki}} \end{aligned} \tag{3.1}$$

Where:

ε_x is the strain in the x

ν_{xy} is Poisson's ratio in the xy direction

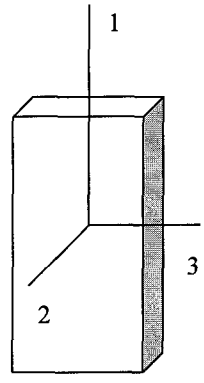

Figure 3.1: Coordinate System

3.1.2 Flexure Data

The material properties that can be determined from the collected flexure data are the maximum flexural stress, the flexure modulus, and the flexural strain at the maximum flexural stress. The load and displacement data of each of the experiments is stored into an array. Once the load and displacement data is recorded the loads are converted to stress and displacements are converted to strain both at the outer surface of the specimen where the values are at their highest. The stress is calculated from equation 3.2 and the strain is calculated from equation 3.3. The maximum flexural stress can easily be obtained from the array of stresses. The flexural modulus can be obtained from the slope of the stress verses strain relation as in the tensile properties.

$$\sigma_f = \frac{3PL}{2bd^2} \tag{3.2}$$

Where:

σ_f is the flexural stress of the outer surface at the midpoint of the specimen,

P is the applied load to the load nose,

L is the support span,

b is the width of the specimen,

d is the depth of the specimen.

$$\epsilon_f = \frac{6Dd}{L^2} \tag{3.3}$$

Where:

ϵ_f is the maximum flexural strain at the outer surface of the specimen,

D is the maximum deflection (at the midpoint) of the specimen.

There is a problem with using equations 3.2 and 3.3 for determining stress and strain. These equations are based on a beam theory that uses the assumption that the beam is isotropic, homogeneous and of equal tensile and compression strengths [18]. From [19] there are assumptions made on the beam's normals, which are imaginary lines that are perpendicular to the neutral plane (the doted line in Figure 3.2). The assumption is that the normals remain straight, unstretched, and remain normal. In bending, one side is in tension and one is in compression, if the material does not respond the same way in compression as in tension the normals would not remain straight. Also with a sandwich type structure the elasticity of the material is likely to be different from one layer to another causing the normals to not be straight as seen in the top of Figure 3.2.

These assumptions do not necessarily eliminate the usefulness of flexure tests on composites. If the effects are small enough they can be considered insignificant, in

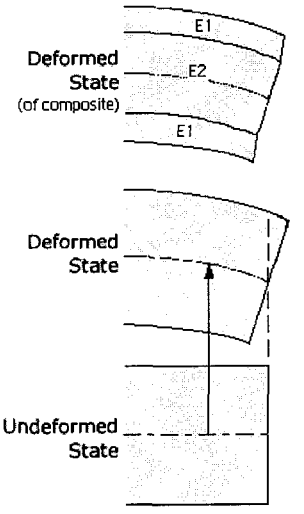

Figure 3.2: Composites Compared to Isotropic Materials for Beam Theory

fact that is the case with isotropic materials. As the composite moves further away from isotropy the worse the assumptions become. Flexure tests are still used in the literature [10, 16, 20, 21] and are useful for comparing properties of composites with varying input factors.

3.1.3 Database Design

After the experimental results are analyzed and the material properties are determined the data must be stored in an easily accessible place. To this end, Microsoft Access was chosen as a database program to store the relevant data. Access records were created to store all the tensile and flexural data from the test coupons. A record is also created with the average results to make an estimate for each of the properties of the original panels. The benefit to using a database program such as Access is that queries can easily be made up in order to sort through all the data and search for whatever criteria the user desires. These query results can be used by Matlab or

Excel and ANOVA can be performed on the necessary data.

3.2 Design of Experiments

Design of experiments (DOE) is a combination of statistical techniques used to choose the values at which the desired experimental factors will be run, give rules on how to run the experiments, and then how to analyze the results. DOE is often used when optimization of a problem is needed. One can determine sensitivities to changes in factors and use DOE for estimating the optimal factor combination from a few tests. In this project an optimum is not of interest because there is nothing specific to optimize. One can use DOE to estimate the sensitivities from a small subset of experiments to determine if all factor combinations must be run, or if some combinations can be eliminated. For good references and examples on DOE see [22–26].

DOE also provides a method of determining whether or not a factor has a significant effect on the response. When looking at raw data sometimes it is difficult to determine what amount of the changes are random error and what is a result of a factor changing. Analysis of variance is a tool to evaluate this problem and will be discussed in the next section.

3.2.1 Analysis of Variance

The core of the DOE analysis is called ANOVA, which is short for analysis of variance. This can be used for determining the effect of a single factor or the effect of multiple factors and their interaction effects. The variance of a population is defined as equation 3.4.

$$\sigma^2 = \frac{\sum(X-\mu)^2}{N} \tag{3.4}$$

Where:

μ is the population mean,

N is the size of the population, and

X is the individual population values.

In order to use equation 3.4, the whole population must be tested. As this is often infeasible, a small sample of the population must be taken and the mean can then be estimated with the sample average. The standard deviation of the sample is an unbiased approximation of the variance of the whole population and is given by equation 3.5.

$$s^2 = \frac{\sum(X-\overline{x})^2}{n-1} \tag{3.5}$$

Where:

$\overline{x}$ is the sample average,

n is the size of the population, and

X is the individual population values.

In equation 3.5 one is subtracted from the sample size n in the denominator in order to make it an unbiased estimate. This is a well examined problem and is explained in many statistics books such as [27].

ANOVA uses the variance of a response from changing a factor and compares it to the variance of the error of the experiment. Using this comparison one can determine if a change in the response is due to the factor the experimenter is trying to test or just due to error in the system. ANOVA is based on equation 3.6. The term $\varepsilon_{(i)j}$ is normally and independently distributed with an average of 0 and a variance σ^2. This is one reason design of experiments states that the experiments should be run in a

random order. If the experiments are not run in a random order the error will not have a normal distribution.

$$y_{ij} = \mu + F_i + \varepsilon_{(i)j} \tag{3.6}$$

Where:

y_{ij} is the response of the i^{th} factor level and j^{th} experiment repeat of that factor level,

μ is the overall mean,

F_i is the effect factor that was varied has on the mean,

$\varepsilon_{(i)j}$ is the random error of the j^{th}repeat in the i^{th} factor level. [23]

The variance is used to check the closeness of the data to this assumption. First the factor sum of squares (SSF) is found using equation 3.7 and then the error sum of squares (SSE) is found using equation 3.8.

$$CT = \frac{1}{IJ}(\sum_{i=1}^{I}\sum_{j=1}^{J} X_{ij})^2 \tag{3.7}$$

$$SSF = \sum_{i=1}^{I}\frac{1}{n}(\sum_{j=1}^{J} X_{ij})^2 - CT$$

$$SST = \sum_{i=1}^{I}\sum_{j=1}^{J} X_{ij}^2 - CT \tag{3.8}$$

$$SSE = SST - SSF$$

In equation 3.7 the correction term CT is introduced. It allows for the deviation around the mean and is given a special designation because it is used for calculating the each sum of squares. In equation 3.8 the SST term is introduced, this is the total

sum of squares. Using this notation the equations can be expanded to a multiple factor ANOVA which is demonstrated in section 4.2.2 of this thesis.

After the sum of squares are found, the mean squares can be calculated by dividing the sum of squares by the degrees of freedom minus 1. This is displayed in equation 3.9, where MSF is the factor mean squares and MSE is the error mean squares.

$$MSF = \frac{SSF}{I-1} \qquad MSE = \frac{SSE}{IJ-1} \tag{3.9}$$

The ratio of the factor mean squares and error mean squares can then be compared to the appropriate F value which is discussed in the next section. If the ratio is larger than the F value the factor is significant. This means the variation in data when the factor level is changed is larger than the variation in error throughout to whole experiment.

3.2.2 Multiple Factor Analysis of Variance

When dealing with more than one factor in an analysis of variance, instead of analyzing each factor individually the data can be analyzed with multiple factors at once. This is beneficial because it can bring to light interaction effects. Interaction effects let the experimenter know how a change in one factor effects the response to a change in another factor. So if one factor interacts with another then when one factor is increased the response when the other factor is changed will change at a different rate.

The principles for the the multiple factor ANOVA is the same as for the single

factor version. The sum of squares is calculated for each factor effect as well as the sum of squares for the interaction effects. These are then divided by their respective degrees of freedom to obtain the mean squares. The mean squares of an effect is divided by the mean squares of error to obtain the F value to determine significance. An extensive example is given in section 4.2.2 of this thesis.

3.2.3 F Value

The F distribution is a probability distribution that is based on two different degrees of freedom. This is a good distribution for comparing factor effects with error effects. The F value is determined by the two separate degrees of freedom and by the level of certainty α. F can be found in tables or can be calculated from the ratio of two chi-squared variables given in equation 3.10 [27].

$$F = \frac{\chi_1/\nu_1}{\chi_2/\nu_2} \tag{3.10}$$

Where:

ν is the number of degrees of freedom,

χ is the chi-squared distribution.

3.2.4 Confidence Interval

The spread in raw data of any specific material property examined in this thesis is large relative to most isotropic materials due to the macroscopic differences in material composition of composites. Therefore one cannot give average of the tests as the definite value of that property for a given panel. It is much more accurate to give a range in which the property value will fall. This range is centered around the

average and the size of the range is based on the spread of the data, or the standard deviation. This is what the confidence interval is used for.

With a confidence interval the experimenter can specify a certainty level α and using the sample average, standard deviation, and the student's t distribution can determine a range in which the actual mean will fall. To compute the confidence interval equation 3.11 is used.

$$\overline{x} - t_{\alpha,\nu} s_{\overline{x}} < \mu < \overline{x} + t_{\alpha,\nu} s_{\overline{x}} \tag{3.11}$$
$$s_{\overline{x}} = \frac{s}{\sqrt{n}}$$

Where:

$t_{\alpha,\nu}$ is the student's t distribution with ν

degrees of freedom and a certainty level of α [23]

In this thesis, Poisson's ratio in the 23 direction is not measured directly. It is calculated from the 12 and 13 directions. In order to determine the confidence interval for the 23 direction since the confidence interval cannot be determined directly, error propagation tools must be employed. For both addition and subtraction the intervals can be added directly. For multiplication and division the absolute error must be added. This involves dividing the interval by the mean as seen in equation 3.12 [28].

$$\Delta z = z\sqrt{\left(\frac{\Delta x}{x}\right)^2 + \left(\frac{\Delta y}{y}\right)^2} \tag{3.12}$$

3.2.5 Box Plots

Box plots can offer a quick visual comparison of data sets. Some trends can be easily determined from the plot. The definition of a box plot is taken from [27,29] and is as follows: In a box plot, each data set is represented by a box with its upper and lower edges on the one quarter and three quarters percentile of the data. A line through the box represents the median of the data. Lines extending from the box represents the upper and lower limit of the data. Outliers, or data that is outside of the upper and lower limits are marked with an asterisk. The quarter percentiles are the median of the largest and smallest n/2 observations, or (n+1)/2 if there is an odd number of observations. The upper and lower limits are a distance of 1.5 times the distance between the one quarter and three quarters percentile away from the box ends. In section 4.1.3 box plots are used to observe the effects of orientation on the composite properties.

3.3 Methods of Modeling

In the results section of this thesis, two methods of modeling are used in an attempt to create a way of predicting material properties. This section outlines the theory behind the models used in the results section. There are many published works on modeling of composite materials, [7, 9, 30–33] many are based on the rule of mixtures method and are just expansions on the theory using more information on the composite and its constituents than is known for the materials in this thesis.

3.3.1 Curve Fitting

Curve fitting can be performed on the experimental data to obtain an empirical equation for the material properties. To do this the results were set up in a matrix form in Matlab and solved by using the method in equation 3.13. These curve fitting methods were taken from [34–36].

$$Y = \beta_0 + \beta_1 X_1 + \beta_2 X_2 + ... + \beta_n X_2^m \tag{3.13}$$

Where:

β_n are coefficients to be determined

Y is the response value

X_1 and X_2 are the factor input levels

Equation 3.13 can be written in matrix form, as in equation 3.14, to be used with many input and response levels.

$$\begin{bmatrix} y_1 \\ \vdots \\ y_n \end{bmatrix} = \begin{bmatrix} x_{11} & \dots & x_{1m} \\ \vdots & \dots & \vdots \\ x_{n1} & \dots & x_{nm} \end{bmatrix} \cdot \begin{bmatrix} \beta_1 \\ \vdots \\ \beta_m \end{bmatrix} \tag{3.14}$$

The matrix equation 3.14 can also be written in the form of equation 3.16. By simply multiplying by the inverse of the factor input levels matrix the vector of coefficients can be found (equation 3.16). Unfortunately this only works for if X is a square, invertible matrix. If this is not the case Matlab uses a least squares approach to solving the system of equations [36].

$$Y = [X]\beta \tag{3.15}$$

$$\beta = Y[X]^{-1} \tag{3.16}$$

3.3.2 Rule of Mixtures

The rule of mixtures uses the separate phases that go into creating a composite in order to estimate the composite properties. It is a very basic model and is good for a very simple approximation of some material properties. This method works on the theory that the composite properties are simply the constituent properties added together, each constituent contributing in portion to their volume fraction. Without any modifiers this theory is for continuous unidirectional fibers. The composites used in this thesis contained chopped and randomly oriented fibers of more than one fiber type so the equation must be modified slightly.

Short fibers, for the purpose of modifying the rule of mixtures are defined as any fiber less than the fiber critical length [33]. The critical length is the minimum length a fiber must be in order for the stress to be fully transferred from the matrix to the fiber and thus to be considered continuous in the rule of mixtures model. This length can be estimated using equation 3.17.

$$\frac{l_C}{d} = \frac{\sigma_f}{2\tau} \tag{3.17}$$

Where:

l_c is the critical fiber length

d is the fiber diameter

σ_f is the maximum fiber stress

τ is the interface shear stress

Since the fibers are not all aligned in one direction each of the fiber components must be multiplied by a factor K in order to compensate for the random orientation [30]. This K factor must be determined experimentally. Thus the rule of mixtures model for the composites used in this thesis is 3.18 for elastic modulus and 3.19 for the maximum tensile stress.

$$E_{Composite} = K_c V_c E_c + K_g V_g E_g + V_m E_m \tag{3.18}$$

$$\sigma_{cu} = K s_c V_c \sigma_c + K s_g V_g \sigma_g + V_m \sigma'_m \tag{3.19}$$

Where:

V is the volume fraction of a phase,

E is the Young's modulus of a phase,

Ks is a correction factor for random orientation fibers.

σ is the ultimate strength of a phase, The subscripts are:

c is for the carbon phase,

g is for the E-glass phase,

m is for the matrix Phase,

Composite is the final product of the phases in composite form.

σ'_m is the matrix strength at the failure strain of the fibers. [32]

3.4 Synopsis

This chapter outlines the theory behind the design and analysis of of the experiments. After the data was collected it was analyzed using a Matlab script and the relevant data was stored in an Access database. Significant effects can be determined numerically using analysis of variance or visually by plotting the data using a box plot. Two models are presented in this chapter: The rule of mixtures is a simple and well known model that uses the properties of the composite's constituents to predict the final composite properties. The curve fitting models are soley based on the experiment results. The curve fitting method is beneficial because it can be used on all the material properties. The rule of mixtures is used for only tensile modulus and maximum tensile stress. The next chapter presents the actual results of the experiments.

Chapter 4

Experimental Results

The primary concern with the planned experiment when the panels came back from the waterjet cutter was that a few of the samples were not labeled or the numbers were almost completely cut off due to poor panel alignment when the cutting occurred. Thus, the original position the of sample on the panel was not certain. The only panels that were not possible to decipher the partial and non-existent numbers were panels 8 and 10. Some of the numbers were visible on panel 10 but none of the numbers were visible for panel 8. In order to make an educated guess as to where the samples came from on the panel, a couple of graphs were created. These graphs can be seen in Figure 4.1, they are plots of sample positions verses sample weights and thicknesses. As seen in the graphs there is a clear pattern as the specimens get toward the middle of the panel they get thicker and more heavy. Using this information, position numbers were chosen for the samples without numbers.

A few samples were lost somewhere during the cutting and were not shipped with the other samples. Of the flexure coupons these were samples 8 and 14 from panel 10 and samples 7, 8, and 13 from panel 3. Also sample 22 from panel 6 of the tensile coupons had been misplaced. The only problem with the missing samples is that

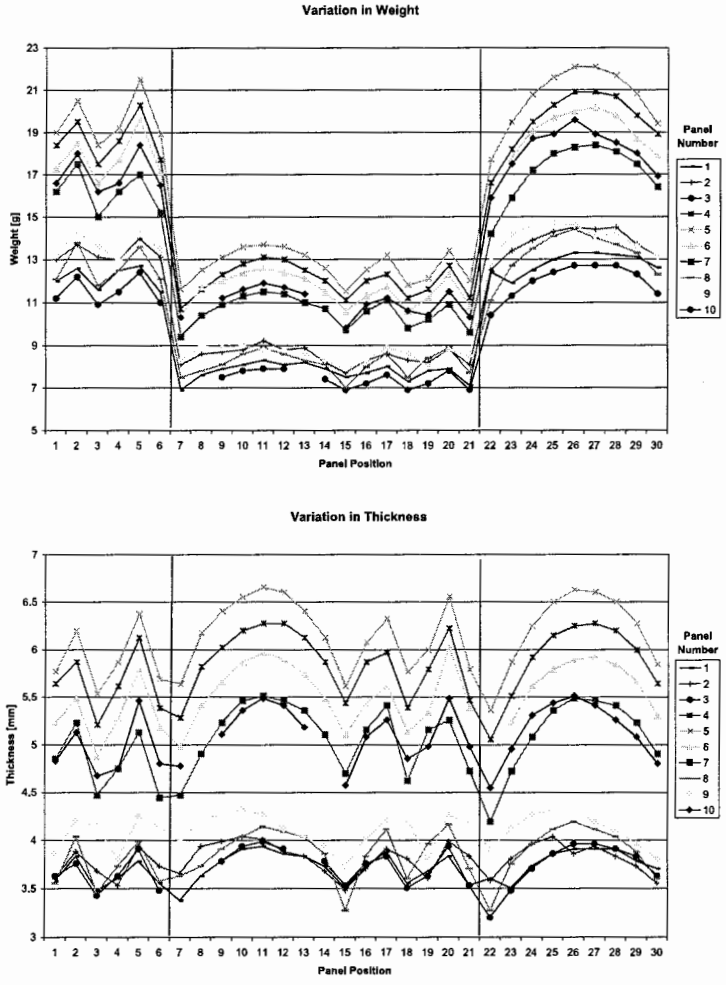

Figure 4.1: Variation of Weight (Top) and Thickness (Bottom) with Panel Position

the panels with missing coupons will not have as many data points to calculate the average, which makes it slightly less likely to be accurate.

After running the tests, there were two samples that produced nonsensical results due to a malfunction in the bi-axial extensometer. The off axis extensometer did not record a displacement change for sample 26 of panel 7 and therefore Poissons ratio could not be determined for that sample. For sample 6 of panel 7 the pins for the axial extensometer were left in, producing results in which only the maximum tensile stress can be used due to the fact the other properties rely on the axial extension measurement.

4.1 Results

The properties of the constituents used in the composites are listed in table 4.1. These properties are used throughout the results section. The densities are used for calculating volume fractions and the modulus and strength properties are used for the modeling calculations. This table shows that carbon fiber is about half the weight of E-glass while it is about three times as stiff and 1.4 times stronger in tension, but E-glass is less brittle and breaks at a strain twice as high as carbon.

Phase	Density $[g/cm^3]$	Tensile Modulus [GPa]	Tensile Strength [MPa]	Yield Elongation [%]
E-Glass [37]	2.54	72.4	3,448	4.8
Carbon [38]	1.80	230	4,900	2.2
Matrix [39]	1.25	3.4	0.083	5.8

Table 4.1: Phase Properties

Table 4.2 is a table of measurements made prior to the experiments being performed. The panel volume was found by multiplying the panel length by the panel width and multiplying by the average specimen thickness for that panel. The density

was then found by dividing the panel weight by the volume. The Core+E-glass weight column is the weight of the Hi Flow mat and the weight of any chopped E-glass added to the Hi Flow mat is given after the '+' sign.

Table 4.2 shows that for the most part the core weight stays relatively constant while the amount of carbon added changes and panel thickness changes.

Panel	Core+E-Glass Weight [g]	Side 1 Carbon Weight [g]	Side 2 Carbon Weight [g]	Panel Weight [g]	Specimen Thickness [mm]	Density [kg/m^3]
1	166+30	70	70	842	3.72	1307
2	156+84	94	94	910	3.81	1366
3	160	0	0	802	3.73	1221
4	163	57	55	1261	5.83	1258
5	159	78	78	1361	6.14	1254
6	158	100	105	1232	5.52	1273
7	170	60	66	1129	5.05	1259
8	168	60	69	868	3.85	1307
9	156+30	70	70	933	4.10	1303
10	142+84	94	94	1182	5.10	1317

Table 4.2: Panel Properties

The mass fractions were calculated by dividing the mass of each phase by the mass of the finished composite panel. The mass fraction for E-glass was found using the chopped E-glass and the mass of the Hi Flow mat. This is making the assumption that the polypropylene in the core of the mat can be approximated by E-glass properties. The total panel weight was measured after the panel edges were trimmed because there is excess resin on the panel after molding. There is a chance that some of the fibers were cut out which would make the mass fractions and volume fractions slightly inaccurate. Regardless, it is not believed that this would change the values by a significant amount. The fiber mass fractions are relatively low in these experiments. The low viscosity of the hybrid resin allows for fiber mass fractions up to 75% (using glass fiber) [39]. The mass fractions are low mainly because it is difficult to stop the

fiber that is added to the Hi Flow mat from bunching and moving during the RTM process, even with the low viscosity.

Panel	Percent E-Glass By Weight [%]	Percent Carbon By Weight [%]	Percent Matrix By Weight [%]
1	23.3	16.6	60.1
2	26.3	20.7	53.0
3	20.0	0.0	80.0
4	12.9	8.9	78.2
5	11.6	11.5	76.9
6	12.9	16.6	70.5
7	15.0	11.2	73.8
8	19.3	14.9	65.8
9	19.9	15.0	65.1
10	19.1	15.9	65.0

Table 4.3: Mass Fractions of the Three Phases

The volume fraction is calculated based on the masses of the phases and their respective densities. The volume of a phase can be approximated by dividing the mass by the density. The volume of the composite panel is determined by the dimensions of the panel using an average thickness. The volume fraction is then found by dividing the volume of the respective phase by the total panel volume. The results are presented in table 4.4.

Panel	Percent E-Glass By Volume [%]	Percent Carbon By Volume [%]	Percent Matrix By Volume [%]
1	25.1	12.1	62.8
2	26.5	15.7	57.9
3	21.8	0.00	78.2
4	15.1	6.21	78.7
5	14.9	8.00	77.1
6	16.4	11.8	71.8
7	17.9	7.8	74.3
8	20.4	10.8	68.8
9	21.3	10.9	67.8
10	19.9	11.6	68.5

Table 4.4: Volume Fractions of the Three Phases

The next two sections will present and discuss the experimental results.

4.1.1 Tensile Results

The following Figures 4.2-4.6 are plots of the tensile stress verses strain of each of the samples. The average tensile modulus is represented by the black line. The black horizontal line represents the average maximum stress level. The red lines on the plots are the samples in the horizontal direction and the blue lines in the vertical direction of the panel. The figures all have the same scale in order to easily see differences between graphs.

These graphs show the variation in the collected data. The graphs also show how the stress strain curves are highly linear until breakage occurs. All specimens result in a brittle fracture. Upon visual inspection it appears that the blue lined data in general might have a higher tensile modulus. In some panels the maximum stress appears higher in the red lines, and some higher in the blue. These orientation effects are further explored in section 4.1.3 of this chapter. In the graphs if the curve makes a sudden jump backward in strain this indicates the extensometer pins slipping on

the specimen surface. Typically this is due to the vibration from the initial cracking that dislodges the pins from their original seated location.

The effects of adding carbon fiber can be seen by comparing panel 3 to the rest of the panels. The tensile modulus for panel 3 is the lowest of all panels. The addition of carbon fiber increases the panel stiffness. The elongation at break is also the highest in panel 3, which is a property of glass composites. As for maximum tensile stress the only panel that was lower than panel 3 was panel 4. This is due to the fact only a small amount of carbon fiber was added, and the thickness was increased. A thickness increase without much fiber added causes the matrix volume fraction to increase and the E-glass volume fraction to decrease. As seen in table 4.4, panel 4 has the largest matrix volume fraction and lowest E-glass volume fraction. Also, the low amount of carbon added caused some samples to have sections that contained no carbon on one side, thus essentially making a local volume fraction of carbon equal to zero and thus lowering the composite strength.

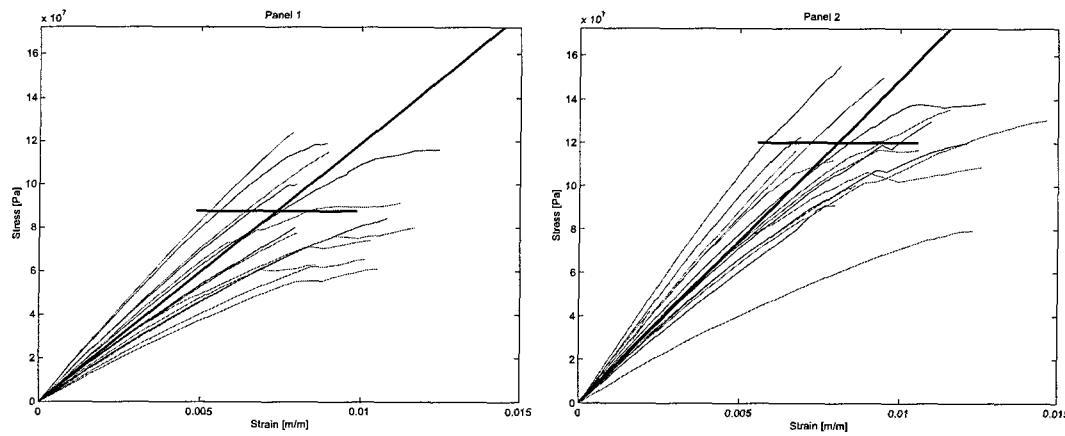

Figure 4.2: Tensile Stress-Strain Plots for Panels 1 and 2

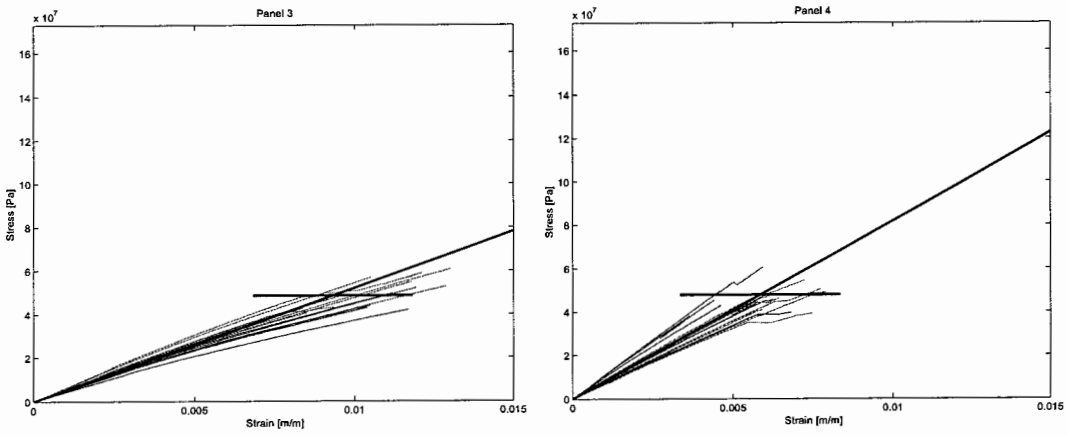

Figure 4.3: Tensile Stress-Strain Plots for Panels 3 and 4

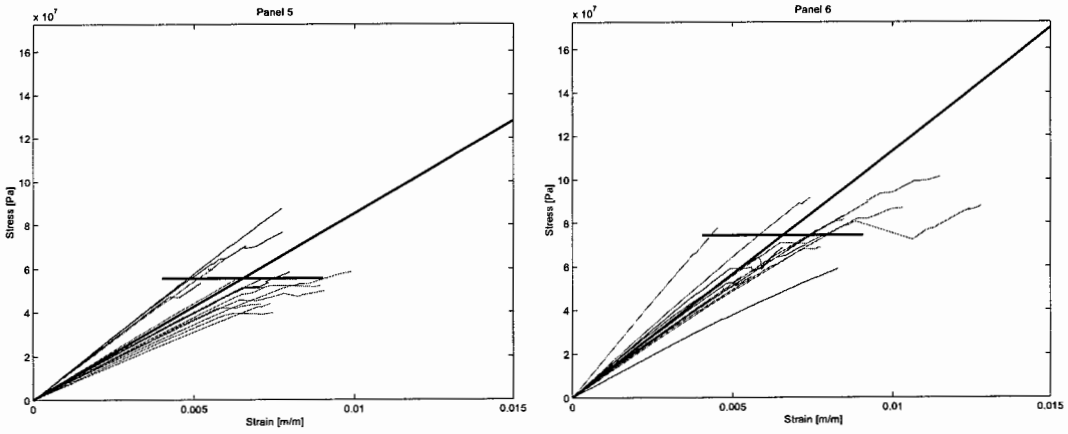

Figure 4.4: Tensile Stress-Strain Plots for Panels 5 and 6

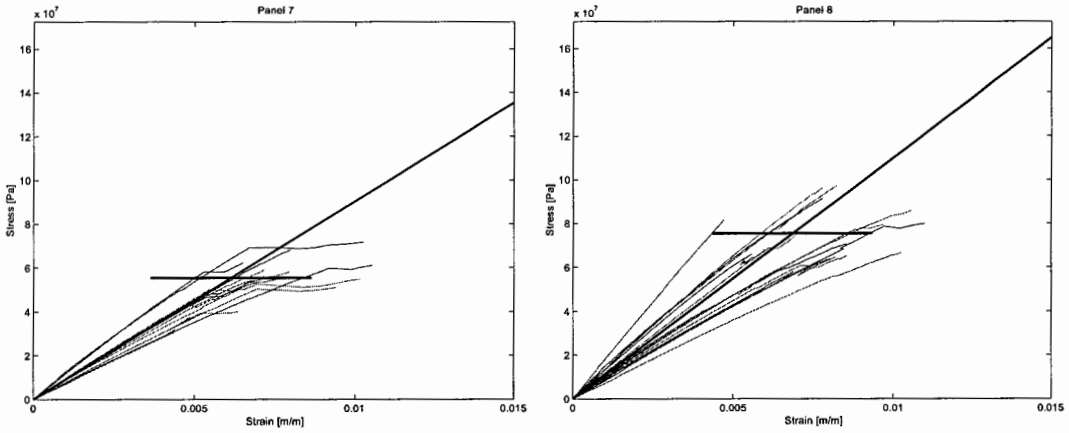

Figure 4.5: Tensile Stress-Strain Plots for Panels 7 and 8

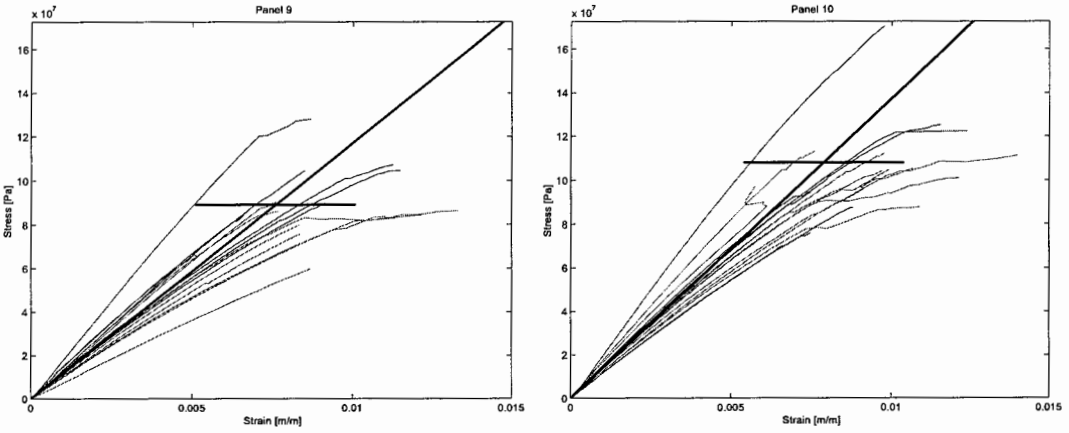

Figure 4.6: Tensile Stress-Strain Plots for Panels 9 and 10

The following Figures 4.7-4.11 are the strain-strain graphs used for determining the Poisson's ratio for the samples. In the figures below the blue lines are the strain in the axial direction plotted against strain in the thickness direction (ν_{12}). The red lines are the strain in the axial direction plotted against strain in the width direction (ν_{13}).

As seen in the graphs, Poisson's ratio is not heavily influenced by changes in the composite's composition. Also, the differences between ν_{12} and ν_{13} are not too large. In fact, with panel 5 the two averages are almost coincident. As seen in Figure 4.12 ν_{13} is more consistent between panels. In fact given the 95% confidence interval (table 4.6) the range of 0.373 to 0.355 is common for all ten panels. ν_{12} seems to have more variability between panels. Although with the exception of panel 5 and panel 7 the 95% confidence interval includes the range of 0.422 to 0.408 for ν_{12}. When ν_{23} is calculated from ν_{12} and ν_{13} the 95% interval widens because uncertainty of a value that is obtained from two experimental values is going to be greater than that of the individual experimental values. The common accepted value range for eight of the panels with regards to ν_{23} is between 0.933 and 0.836. Once again panel 5 and panel 7 are outside of this range. It can be seen from graph 4.12 that the uncertainty of ν_{13} is less than that of ν_{12}. It is not known what would cause this effect, but it is possibly to do with the surface finishes which are different for the two directions. When measuring the thickness change the finish is mostly smooth but has some surface voids either in the direction of the fibers or between the fibers. As the experiment proceeds the extensometer pins locate these surface voids and cause erratic effects as the pins slip into the voids. When measuring in the width direction the surface is that which is left from the water jet cutter. It is more rough than the resin surface but also it is more consistent.

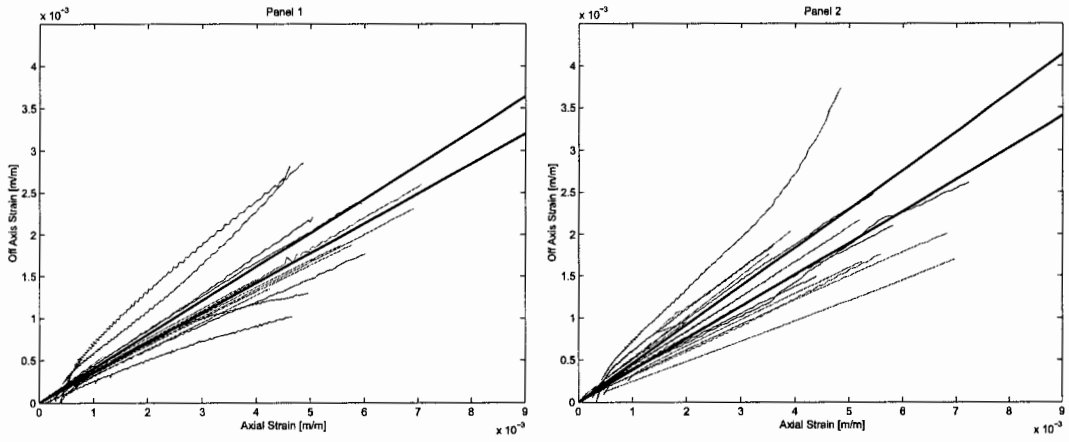

Figure 4.7: Tensile Strain-Strain Plots for Determination of Poisson's Ratio of Panels 1 and 2

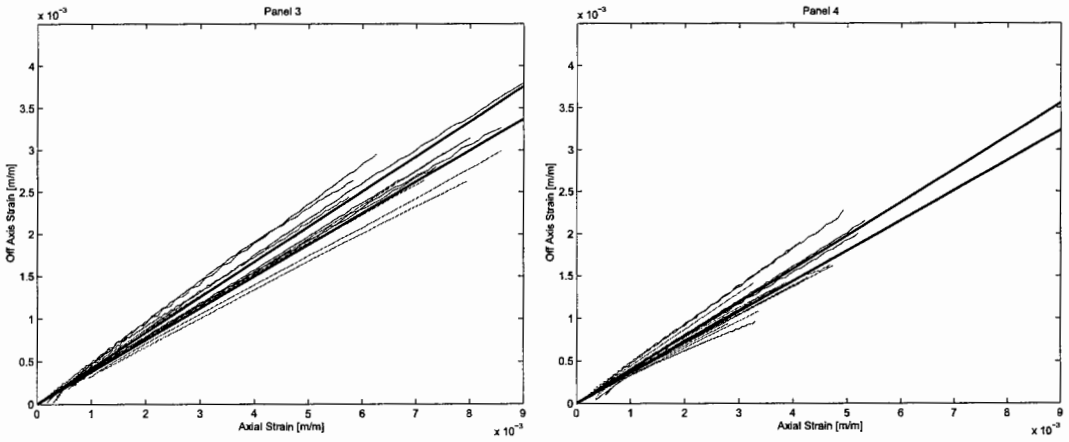

Figure 4.8: Tensile Strain-Strain Plots for Determination of Poisson's Ratio of Panels 3 and 4

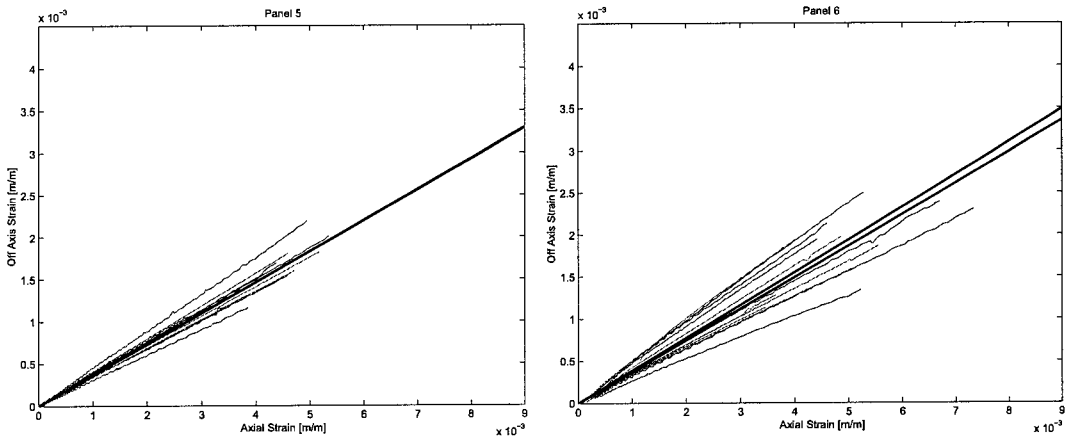

Figure 4.9: Tensile Strain-Strain Plots for Determination of Poisson's Ratio of Panels 5 and 6

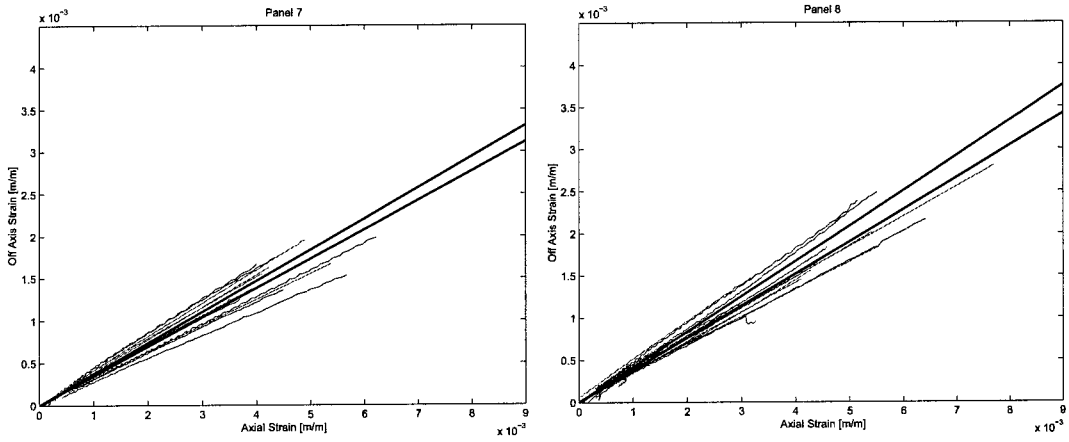

Figure 4.10: Tensile Strain-Strain Plots for Determination of Poisson's Ratio of Panels 7 and 8

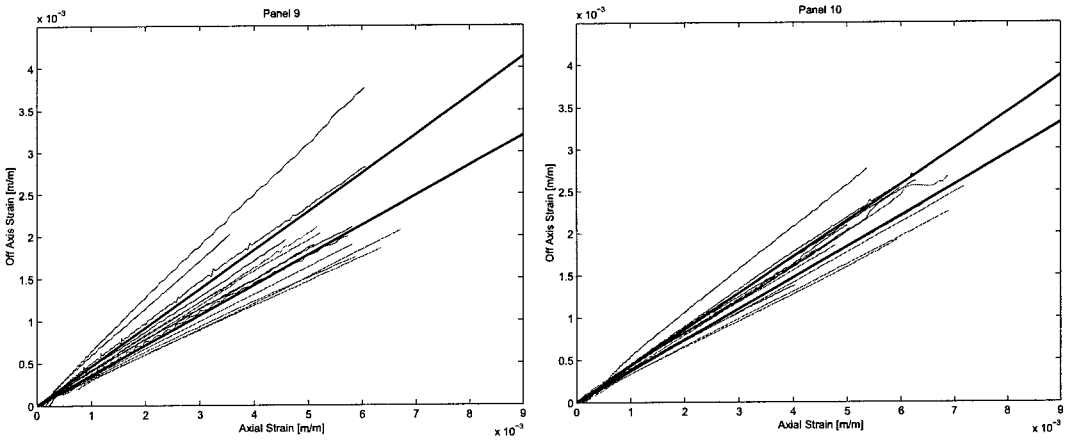

Figure 4.11: Tensile Strain-Strain Plots for Determination of Poisson's Ratio of Panels 9 and 10

Table 4.5 is a list of the averaged tensile results.

Panel	Tensile Modulus [GPa]	Maximum Tensile Stress [MPa]	ν_{12} [m/m]	ν_{13} [m/m]	ν_{23} [m/m]	Tensile Strain at Maximum Stress [%]
1	11.9	87.6	0.404	0.356	-1.14	0.937
2	14.9	120	0.460	0.379	-1.21	1.04
3	5.20	48.5	0.417	0.375	-1.11	1.09
4	8.16	47.7	0.395	0.359	-1.10	0.655
5	8.52	55.5	0.367	0.366	-1.00	0.721
6	11.3	74.1	0.388	0.373	-1.04	0.798
7	9.01	55.3	0.346	0.368	- 0.942	0.789
8	11.0	75.2	0.417	0.380	-1.10	0.821
9	11.7	88.9	0.459	0.355	-1.29	0.934
10	13.7	108	0.430	0.368	-1.17	0.991

Table 4.5: Tensile Panel Properties

Table 4.6 is a table of the 95% confidence levels for their respective properties for each panel.

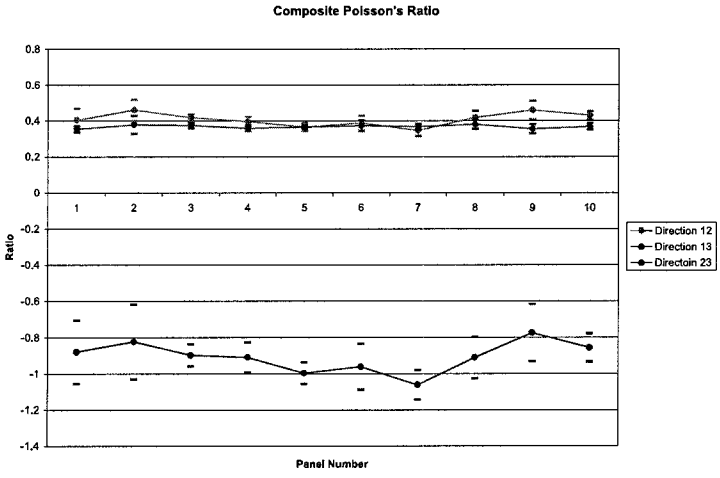

Figure 4.12: Confidence Interval of Poisson's Ratio

Panel	Tensile Modulus [GPa]	Maximum Tensile Stress [MPa]	ν_{12} [m/m]	ν_{13} [m/m]	ν_{23} [m/m]	Tensile Strain at Maximum Stress [%]
1	(13.2, 10.6)	(97.7, 77.6)	(0.467, 0.341)	(0.373, 0.338)	(-1.06, -0.704)	(1.04, 0.830)
2	(16.1, 13.7)	(130, 111)	(0.519, 0.401)	(0.428, 0.330)	(-1.03, -0.617)	(1.15, 0.928)
3	(5.42, 4.97)	(51.7, 45.2)	(0.436, 0.398)	(0.389, 0.360)	(-0.959, -0.836)	(1.16, 1.02)
4	(8.74, 7.58)	(50.6, 44.7)	(0.422, 0.368)	(0.375, 0.343)	(-0.992, -0.827)	(0.707, 0.603)
5	(9.24, 7.79)	(61.4, 49.7)	(0.389, 0.345)	(0.374, 0.358)	(-1.06, -0.937)	(0.779, 0.663)
6	(12.3, 10.3)	(81.1, 67.0)	(0.428, 0.347)	(0.402, 0.344)	(-1.07, -0.835)	(0.905, 0.691)
7	(9.70, 8.31)	(60.0, 50.7)	(0.376, 0.316)	(0.382, 0.353)	(-1.14, -0.980)	(0.869, 0.698)
8	(12.3, 9.70)	(81.4, 69.0)	(0.454, 0.380)	(0.405, 0.355)	(-1.03, -0.798)	(0.910, 0.731)
9	(12.7, 10.7)	(96.5, 81.3)	(0.510, 0.408)	(0.380, 0.331)	(-0.933, -0.617)	(1.03, 0.838)
10	(14.5, 13.0)	(117, 97.7)	(0.453, 0.407)	(0.386, 0.351)	(-0.935, -0.779)	(1.09, 0.891)

Table 4.6: Confidence Interval for Tensile Properties

Using the data from each successful test, equations 4.1a through 4.1c were obtained as an empirical model for the material properties listed. Each equation is a special cubic with each individual factor and their interactions represented, but no squared or cubed terms are present. The orientation, O, was set as 1 for vertical samples and -1 for horizontal samples. C and G are the volume fractions of carbon and E-glass fibers respectively. The matrix volume fraction is not included as a factor because it is linearly dependant on C and G.

The equations are useful for calculating material properties within the experimental factor range. The model should not be used to calculate properties much outside the experimental range of the factors. This is know as extrapolation, and when extrapolating far from observation limits, the model can be very poor as described in [27]. One example of this is that the model can be used to determine the properties of a composite that has a high fiber volume fraction. This would give high values for each of the properties, but when it came time to make the composite, it would be impossible to completely wet out the fibers and there would be large dry spots, causing properties much lower than predicted.

Tensile Modulus :

$$\begin{aligned} y =& 0.46 + 3.69\,O + 84.93\,C + 21.19\,G - 31.61\,OxC - 16.74\,OxG \\ & - 107.70\,CxG + 159.15\,OxCxG\ GPa \end{aligned} \tag{4.1a}$$

Maximum Tensile Stress :

$$\begin{aligned} y =& -49.51 + 24.26\,O + 734.39\,C + 432.22\,G - 323.47\,OxC - 108.32\,OxG \\ & - 1525.04\,CxG + 1546.97\,OxCxG\ MPa \end{aligned} \tag{4.1b}$$

Strain at Maximum Tensile Stress :

$$y = -4.01 - 0.09\,O + 58.34\,C + 66.83\,G - 17.29\,OxC + 2.20\,OxG - 314.79\,CxG + 48.42\,OxCxG\ mm/m \tag{4.1c}$$

Where:
O is the orientation, given a value of 1 for vertical and -1 for horizontal
C is the volume fraction of carbon
G is the volume fraction of E-glass

4.1.2 Flexural Results

The following Figures 4.13-4.17 are the plots from which the flexure data was obtained. Looking at the graphs it is interesting to note that the panels with the lowest percentage of carbon have very little residual strength after the coupon reaches it's peak stress. Panels 3, 4, 5, and 7 have the lowest carbon percentage and their figures show a sharp drop down to a very low stress after the peak. The other figures show, at least some of the time, significant residual strength after failure. Panel 2 has the highest carbon volume fraction and has some of the most significant residual strengths of any of the samples.

Panel 3 has the lowest average flexural modulus and maximum stress and the highest strain at maximum stress. This is not surprising, since the outer surfaces are solely composted of E-glass fibers (and the stitching of the mat). Due to the nature of the applied load in flexure testing, the maximum stresses and strains occur at the surface of the specimen. The top surface is in compression and the bottom surface is in tension and half way through the specimen is the neutral axis where the axial load is zero. Thus the material at the surfaces carry most of the load. Since carbon fiber

is added to the specimens on the surface, the addition of carbon drastically increases the rigidity of the material.

In one of the next stages of testing for this project impact of plates using a drop-weight tester will be performed. With this type of impact test the plate is supported around it's edges and the weight is dropped onto the middle. This loading scheme is most similar to the flexure testing. The residual strengths seen in the graphs of the flexure results may be representative of residual strengths after impact. Thus the higher the carbon volume fraction the stronger a sample will be after initial damage occurs.

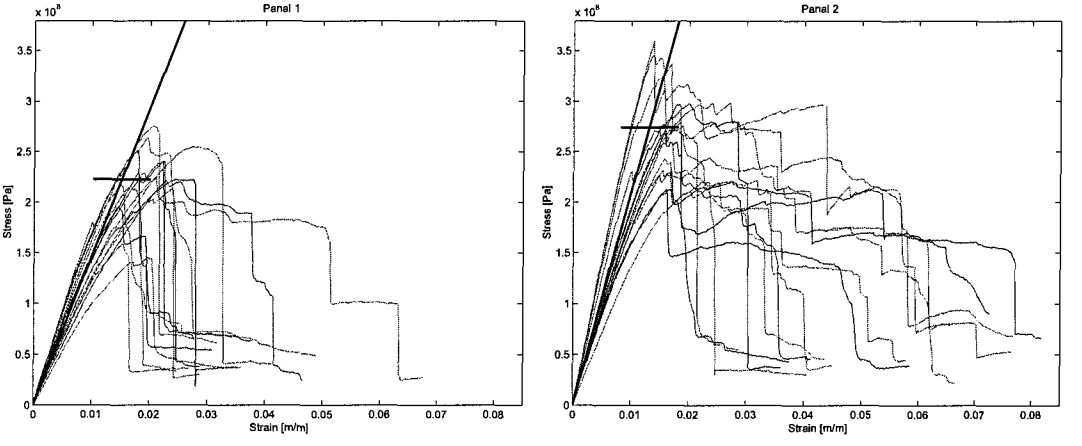

Figure 4.13: Flexure Stress-Strain Plots for Panels 1 and 2

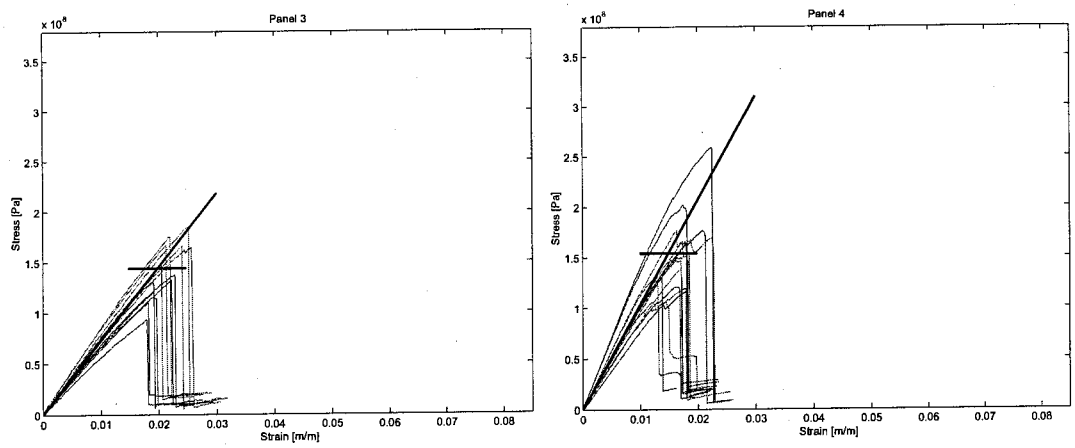

Figure 4.14: Flexure Stress-Strain Plots for Panels 3 and 4

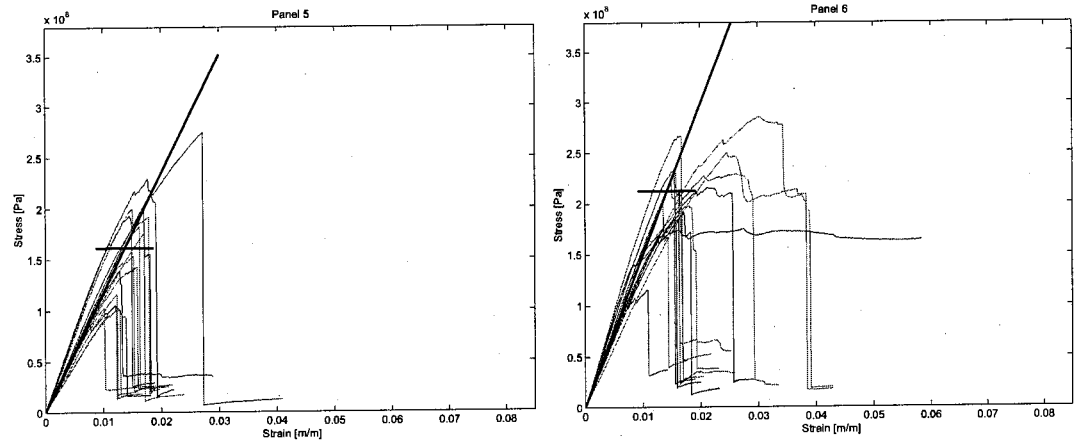

Figure 4.15: Flexure Stress-Strain Plots for Panels 5 and 6

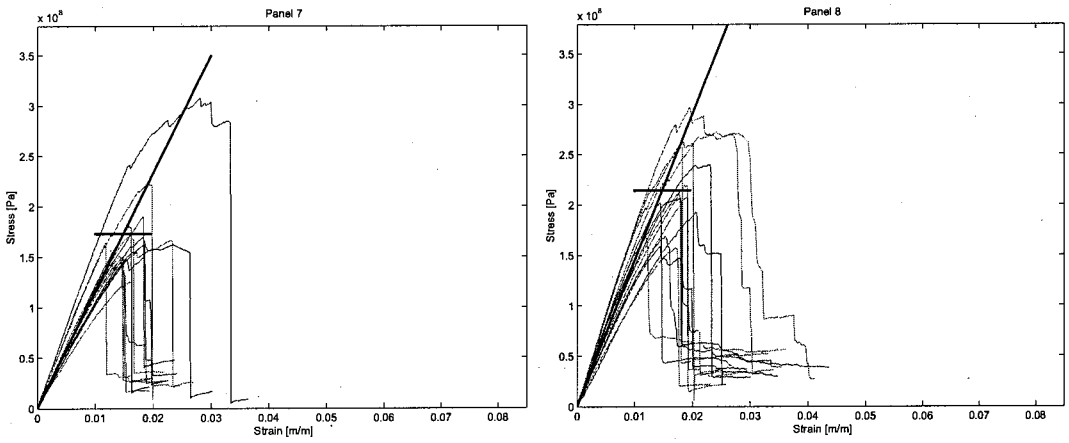

Figure 4.16: Flexure Stress-Strain Plots for Panels 7 and 8

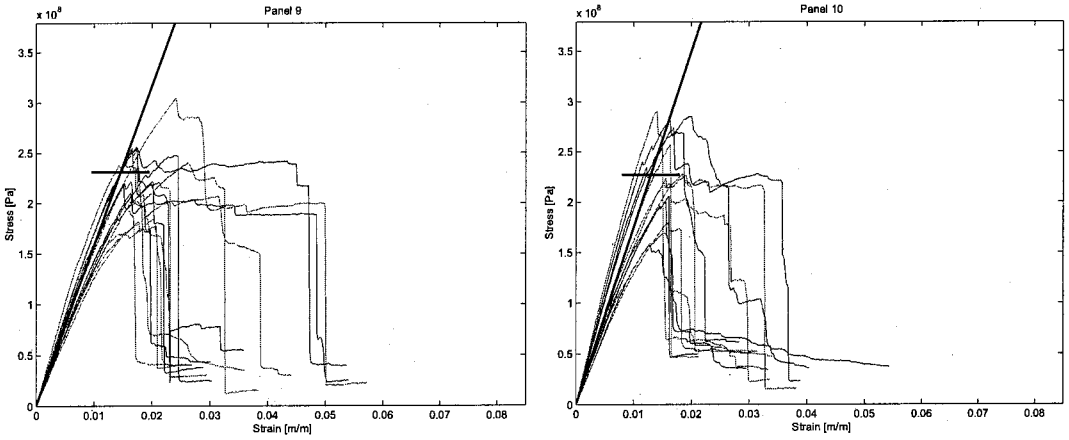

Figure 4.17: Flexure Stress-Strain Plots for Panels 9 and 10

The experimentally obtained values for flexure modulus, maximum stress, and the strain at maximum stress are presented in table 4.7.

Panel	Flexure Modulus [GPa]	Maximum Flexural Stress [MPa]	Flexural Strain at Maximum Stress [%]
1	14.6	222	2.18
2	20.8	274	2.00
3	7.28	144	2.24
4	10.3	154	1.78
5	11.7	161	1.65
6	14.9	212	1.94
7	11.7	173	1.80
8	14.5	214	1.90
9	15.9	231	2.05
10	17.5	227	1.70

Table 4.7: Flexural Panel Properties

Table 4.8 lists the 95% confidence interval for the flexural properties along with the confidence interval for specimen thickness.

Panel	Specimen Thickness [mm]	Flexure Modulus [GPa]	Maximum Flexural Stress [MPa]	Flexural Strain at Maximum Stress [%]
1	(3.82, 3.62)	(15.7, 13.5)	(237, 206)	(2.37, 1.99)
2	(3.91, 3.70)	(22.9, 18.8)	(296, 252)	(2.23, 1.78)
3	(3.86, 3.61)	(7.67, 6.89)	(157, 131)	(2.36, 2.11)
4	(6.07, 5.60)	(11.1, 9.57)	(172, 136)	(1.91, 1.65)
5	(6.37, 5.90)	(12.7, 10.8)	(185, 137)	(1.86, 1.44)
6	(5.73, 5.32)	(15.8, 14.0)	(230, 193)	(2.20, 1.67)
7	(5.29, 4.81)	(12.5, 10.9)	(193, 154)	(1.98, 1.62)
8	(4.02, 3.68)	(15.7, 13.3)	(234, 195)	(2.06, 1.75)
9	(4.21, 3.99)	(16.8, 14.9)	(246, 216)	(2.26, 1.84)
10	(5.29, 4.90)	(19.0, 16.0)	(248, 207)	(1.79, 1.61)

Table 4.8: Confidence Interval for Thickness and Flexural Properties

Using all the data from each successful test, equations 4.2a through 4.2c were obtained as an empirical model for the material properties listed. Each equation is

a special cubic each of the individual factors and their interactions are represented, but no squared or cubed terms are present. The variables have the same definition as those in the models in section 4.1.1.

Flexural Modulus :

$$y = 2.56 + 0.09\,O + 89.68\,C + 18.63\,G + 22.91\,OxC - 1.75\,OxG - 46.35\,CxG - 102.97\,OxCxG\ GPa \quad (4.2a)$$

Maximum Flexural Stress :

$$y = -2.35 + 144.73\,O + 1382.16\,C + 647.68\,G - 1075.72\,OxC - 715.39\,OxG - 2914.72\,CxG + 5057.17\,OxCxG\ MPa \quad (4.2b)$$

Strain at Maximum Flexural Stress :

$$y = 6.23 + 10.80\,O + 51.16\,C + 73.56\,G - 68.31\,OxC - 53.30\,OxG - 330.19\,CxG + 328.37\,OxCxG\ mm/m \quad (4.2c)$$

Where:
O is the orientation, given a value of 1 for vertical and -1 for horizontal
C is the volume fraction of carbon
G is the volume fraction of E-glass

Plastics often have higher flexural properties than tensile properties [37]. For this reason designers often will use the material properties from flexural testing for design instead of tensile testing when a part is subject to a more flexural type load. This increase in flexural properties can be seen in Figures 4.18 to 4.20. The following figures are plots demonstrating graphically the 95% confidence interval. The average is displayed as the solid dots and the upper and lower confidence levels are displayed with a dash. The modulus and maximum stress comparisons demonstrate very similar trends between flexure and tension tests. However the stain at maximum stress comparison does not demonstrate much similarity between the two types of tests. This data would be more useful if the material was a fully isotropic plastic. Due to warnings given earlier in this thesis the flexural results should not necessarily be taken as accurate and thus should not be used for design.

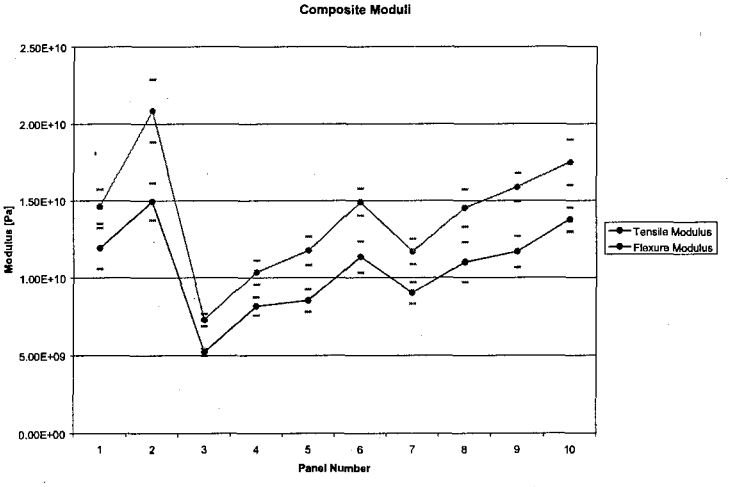

Figure 4.18: Confidence Interval of Tensile and Flexural Moduli

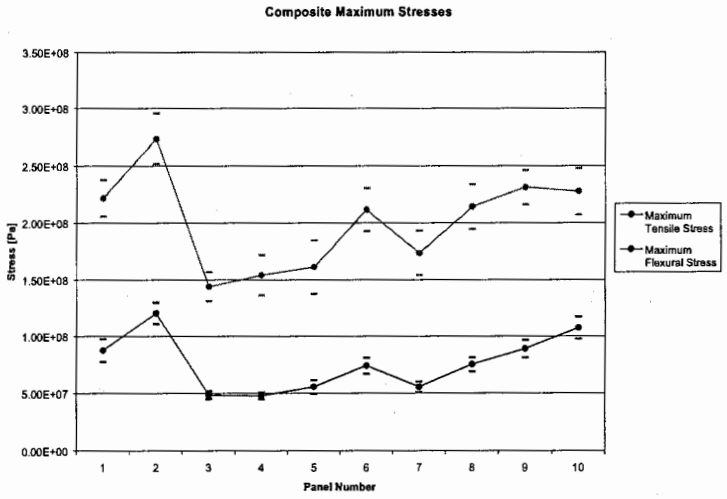

Figure 4.19: Confidence Interval of The Maximum Tensile and Flexural Stresses

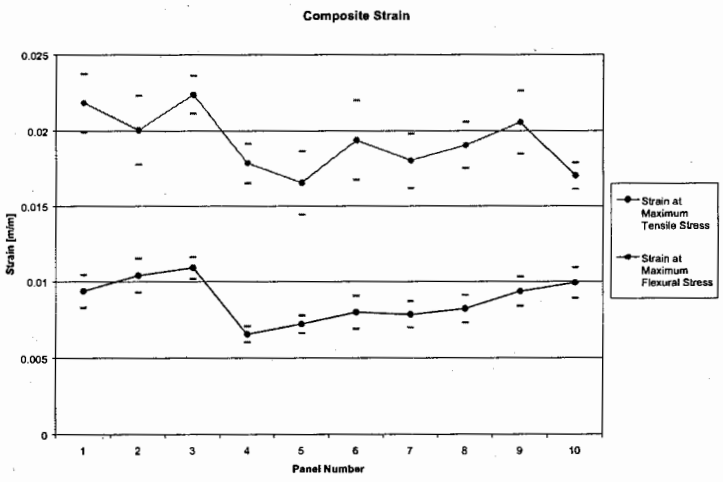

Figure 4.20: Confidence Interval of The Strain at Maximum Tensile and Flexural Stress

4.1.3 Effects of Orientation

Based on an ANOVA of each panel for each property, the orientation significance can be compared to what is seen in each box plot. The ANOVA results can be seen in table 4.9, the box plots are shown in Figure 4.21 through Figure 4.26 (orientation 1 is vertical and 2 is horizontal). The gap between the first and third quarter percentiles is quite substantial in most cases. This makes it impossible to resolve an effect if it is minor. Panel 3 has some of the smallest data scatter. This is likely due to the fact it is just the Hi Flow mat which is manufactured with consistent fiber density and random orientation. When the carbon or glass fiber is added by a human, it can be clumped together and not uniformly distributed. It is likely that the positioning of the horizontal and vertical samples on the original panel can be a major cause of orientation effects. The vertical samples were all at the edge of the panel and the horizontal samples were in the middle. The middle samples are thicker and with even fiber distribution that means there is more resin, giving a lower fiber volume fraction, weakening the sample.

Property	Panel with Significant ANOVA for Orientation
Tensile Modulus	3, 9
Maximum Tensile Stress	6, 7, and 9
Strain at Maximum Tensile Stress	4
Flexural Modulus	3
Maximum Flexural Stress	3, 6
Strain at Maximum Flexural Stress	3, 5

Table 4.9: ANOVA Results for Individual Panels

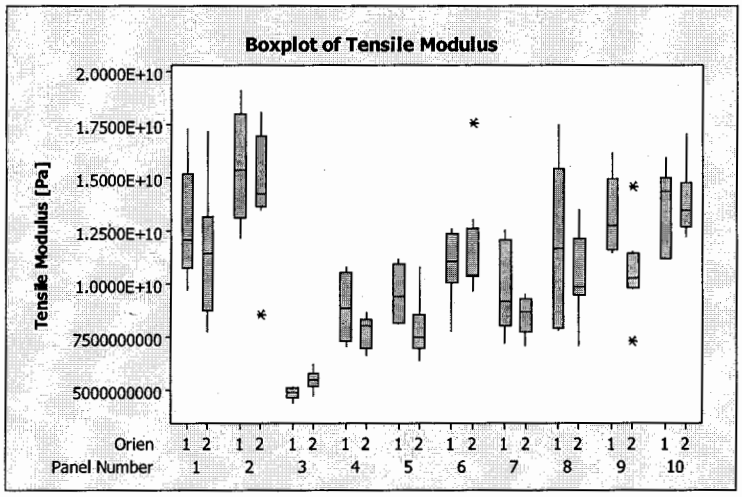

Figure 4.21: Box Plot Orientation Comparison for Tensile Modulus

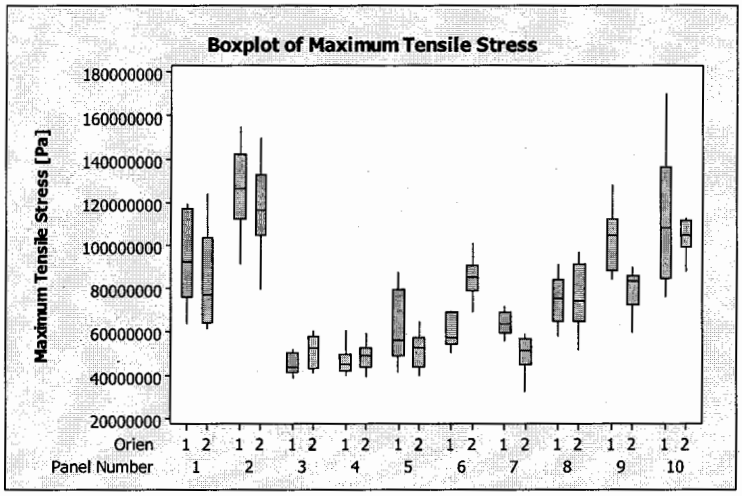

Figure 4.22: Box Plot Orientation Comparison for Maximum Tensile Stress

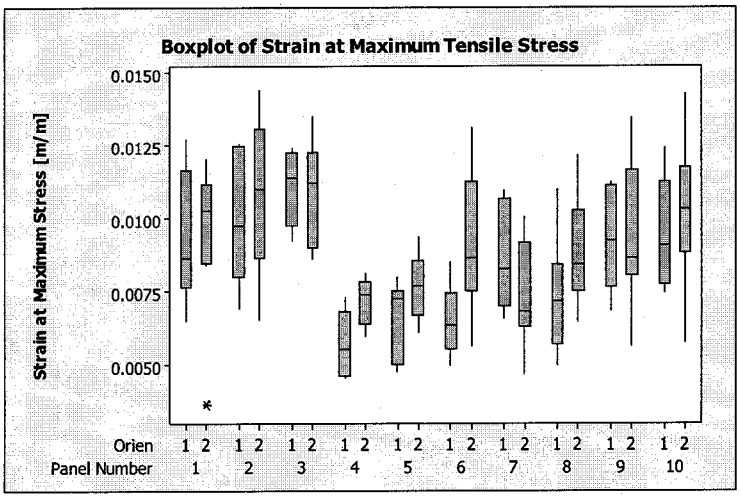

Figure 4.23: Box Plot Orientation Comparison for Strain at Maximum Tensile Stress

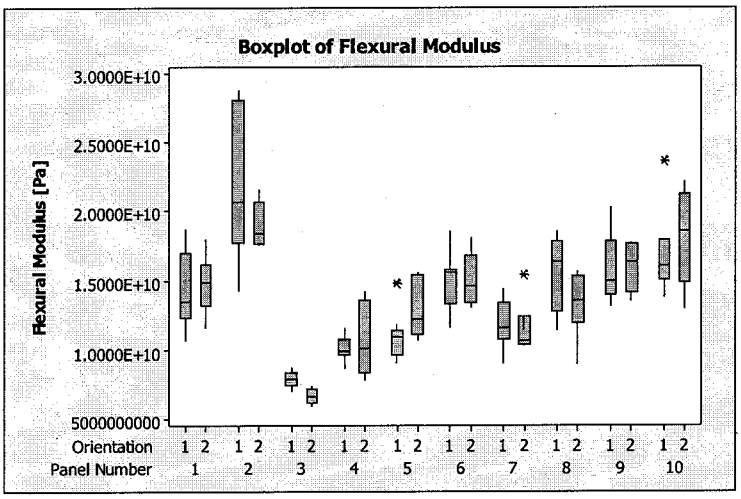

Figure 4.24: Box Plot Orientation Comparison for Flexural Modulus

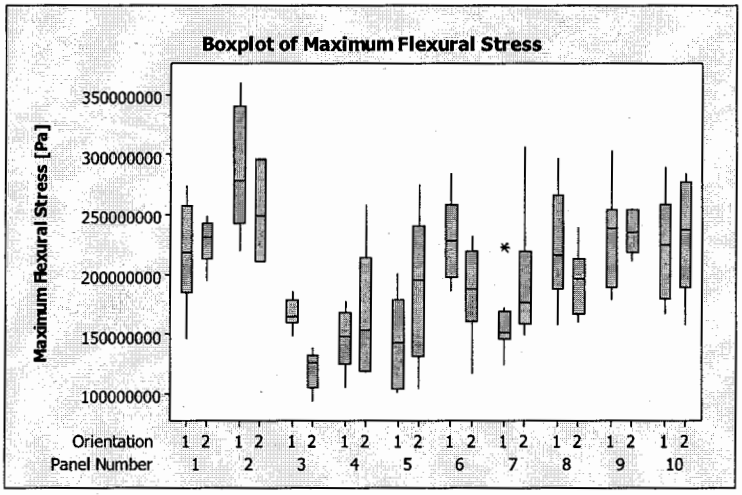

Figure 4.25: Box Plot Orientation Comparison for Maximum Flexural Stress

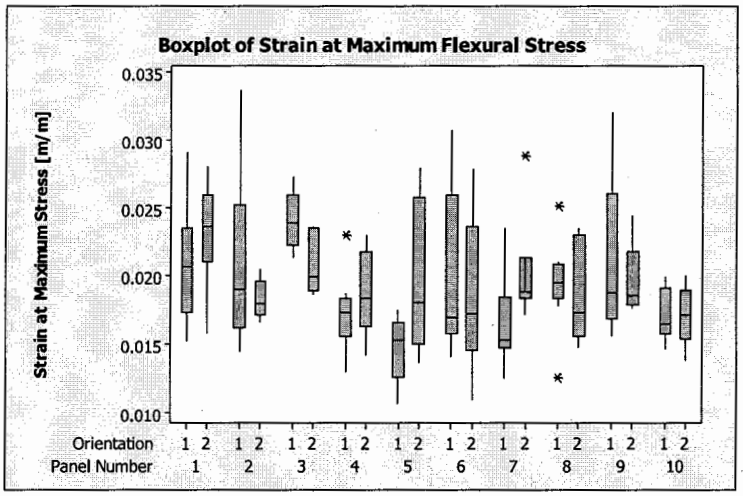

Figure 4.26: Box Plot Orientation Comparison for Strain at Maximum Flexural Stress

From the ANOVA and box plot results panel 3 is the most common to show orientation effects. This is most likely because it consisted of only the Hi Flow mat. The E-glass on the mat is a chopped and in a random orientation on both sides of a core. The core can be seen in Figure 4.27. The chopped glass layers are held to the core by stitching. This stitching is done about half an inch apart and is only in one direction. This would add some directionality to the material properties of the composite. Also some directionality can be seen in the core which is a polypropylene material that is essentially a system of loops. Thus it readily stretches in one direction and not in the perpendicular direction. Once carbon is added to the composite, the carbon properties dominate the composite and most of the orientation effects disappear or become indistinguishable from the noisy data.

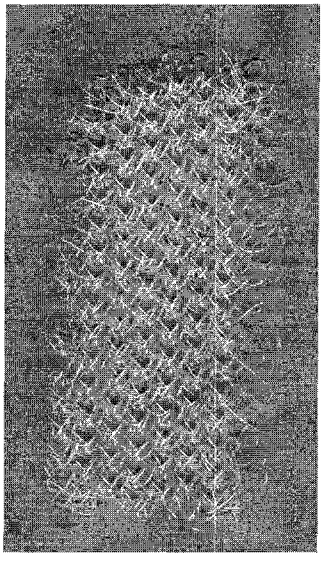

Figure 4.27: Hi Flow Mat Core

4.2 Modeling of Experimental Data

4.2.1 Rule of Mixtures

The fibers used are about 30mm in length. Equation 3.17 is used to calculate whether this length will effect the rule of mixture because it is too short. The term τ is unknown for the fiber and matrix combination used in this thesis but Fu et al. [7] performed experiments on glass and carbon fiber pullouts and found the critical lengths to be 887.92 μm and 813.87 μm respectively. Thus the average fiber length is about 33 times the critical length, so even though the experiments were not conducted with the same matrix, it is safe to assume the majority of the fibers are over the critical length.

Figure 4.28 shows the results of the rule of mixtures comparison with experimental results. The comparison for tensile modulus is very good. The experimental results are shown with the confidence interval included. For the tensile results only the modeled value for panel 10 was not within the confidence limits of the experimental data. For the tensile modulus fit the value for K_c was 0.24 and K_g was 0.17. The fit for the maximum stress properties was not as accurate, the modeled value was outside of the confidence interval for panels 4, 7, and 10. The values used for Ks_c and Ks_g were 0.07 and 0.065 respectively. It is likely that the maximum stress approximations were poor due to the fact that the rule of mixtures only models one failure mode. The mode of failure it models is fiber breakage. The composite can fail in other modes such as fiber pullout or delamination. In fact some combination of these modes are more likely due to the chopped nature of the fibers. This also explains the very low value of Ks_c and Ks_g. The effect of the non continuous fibers is confounded with the random orientation effect.

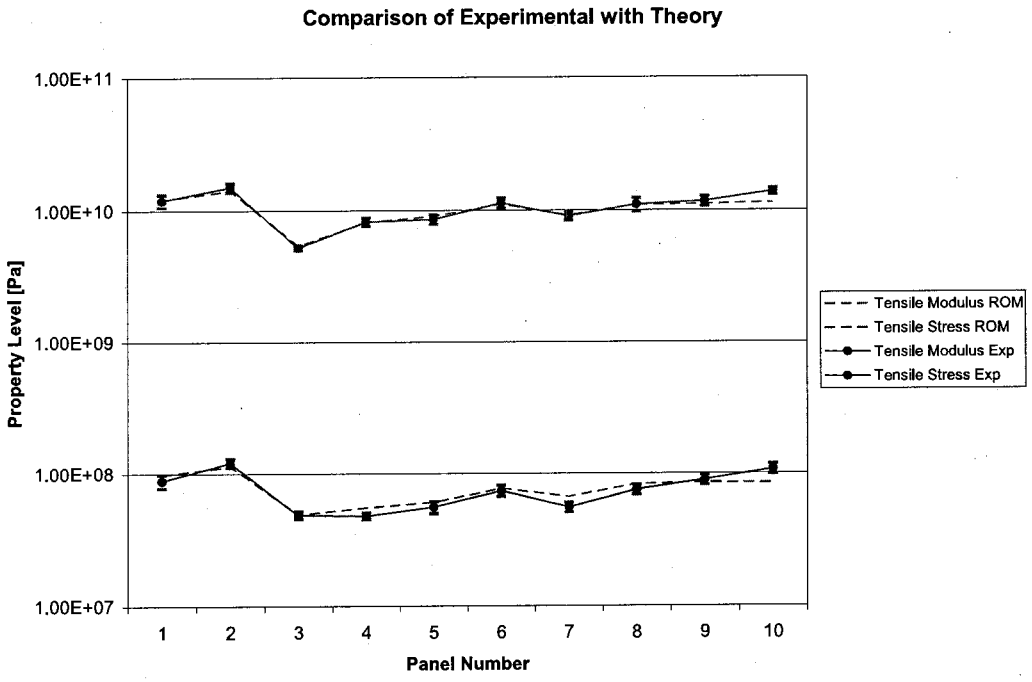

Figure 4.28: Comparison of Rule of Mixtures Estimation With Experimental Data

4.2.2 Analysis of Variance

ANOVA can be carried out in order to determine what factors have a statistically significant effect on the response. To accomplish this at least 4 points must be used, and they should consist of only 2 levels from each factor such that it makes a simple factorial design. Figure 4.29 is a scatter plot of the carbon and E-glass volume fractions of the 10 panels. A factorial design would be represented by a box shape in the plot. The points that are surrounded by the quadrilateral in Figure 4.29 are close to a factorial design but the E-glass volume fraction rises a little when the carbon volume fraction rises. This is a problem because it confounds the effect of E-glass with that of carbon. When the method examines the effect of carbon alone it is not accurate because the E-glass is contributing to the effect as well. Thus the effect of carbon will seem higher than it is in reality. The other problem that is confounded in the results is that the matrix volume fraction does not stay constant between panels, or even between samples in the panels due to thickness variation.

The raw data in the following table is the tensile modulus data (in psi) for panels 5, 6, 7, and 10. Only 5 measurements are used for the data points because panel 7 only had 5 measurements. Thus position 6 was omitted from each panel to keep as consistent as possible.

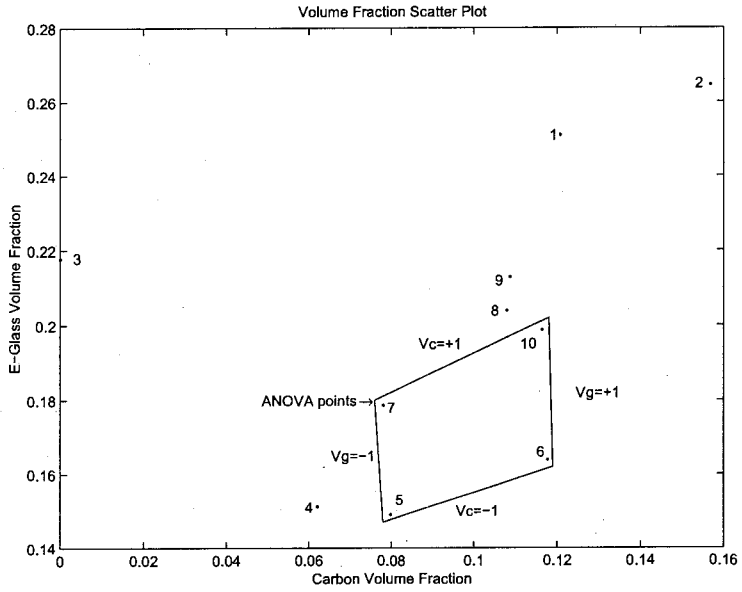

Figure 4.29: Scatter Plot Showing ANOVA Points

			V_g	
		Orientation	+1	-1
V_c	+1	+1	2118372	1564158
			2129324	1825315
			2047249	1787900
			2309260	1592432
			1620189	1122713
		-1	1967820	1506336
			1901825	2541999
			1773726	1501849
			2480527	1640292
			1974019	1396935
	-1	+1	1330293	1542247
			1287782	1185736
			1040898	1623855
			1819631	1180878
			1675320	1171896
		-1	1321056	1299836
			1233305	1569204
			1022998	967003
			1338746	1084765
			1259663	919582

The model used for the ANOVA is listed below. Each of the interactions is examined including the three way interaction. Three way interactions are often left out of ANOVA because their physical meaning is difficult to understand. In this case, leaving it out does not make much difference to the results so it is left in for

completeness.

Model:

$$y_{ijkl} = \mu + C_i + G_j + CG_{ij} + O_k + CO_{ik} + GO_{jk} + CGO_{ijk} + \varepsilon_{(ijk)l}$$

$$i = 1, 2\ j = 1, 2\ k = 1, 2\ l = 1, 2, 3, 4, 5$$

The summation of the responses grouped by each factor (or treatment, T) and combination are listed in the following tables. Dot notation is used in the tables, a dot in place of an index means that the responses have been summed over that index.

Totals:

C		G		O			
$T_{1...}$	36802240	$T_{.1..}$	33652003	$T_{..1.}$	31975448	Total	
$T_{2...}$	25874694	$T_{.2..}$	29024931	$T_{..2.}$	30701486	$T_{....}$	62676934
$\sum_i T^2_{i...}$	2.024E+15	$\sum_j T^2_{.j..}$	1.975E+15	$\sum_k T^2_{..k.}$	1.965E+15	$T^2_{....}$	3.928E+15

C by G		C by O		G by O	
$T_{11..}$	20322311	$T_{1.1.}$	18116912	$T_{.11.}$	17378318
$T_{12..}$	13329692	$T_{1.2.}$	18685328	$T_{.12.}$	16273685
$t_{21..}$	16479929	$T_{2.1.}$	13858536	$T_{.21.}$	14597130
$T_{22..}$	12545002	$T_{2.2.}$	12016158	$t_{.22.}$	14427801
$\sum_i \sum_j T^2_{ij..}$	1.01964E+15	$\sum_i \sum_k T^2_{i.k.}$	1.01381E+15	$\sum_j \sum_k T^2_{.jk.}$	9.88076E+14

The following are the equations to obtain the sum of squares (SS) for each of the treatment conditions.

$$SS_{Total} = \sum_i \sum_j \sum_k \sum_l T^2_{ijkl} - \frac{T^2_{....}}{n}$$

$$SS_{Carbon} = SS_C = \frac{1}{jkl}\sum_i T_{i...}^2 - \frac{T_{....}^2}{n}$$

$$SS_{Glass} = SS_G = \frac{1}{ikl}\sum_j T_{.j..}^2 - \frac{T_{....}^2}{n}$$

$$SS_{CxG} = \frac{1}{kl}\sum_i\sum_j T_{ij..}^2 - \frac{T_{....}^2}{n} - SS_C - SS_G$$

$$SS_{Orientation} = SS_O = \frac{1}{ijl}\sum_k T_{..k.}^2 - \frac{T_{....}^2}{n}$$

$$SS_{CxO} = \frac{1}{jl}\sum_i\sum_k T_{i.k.}^2 - \frac{T_{....}^2}{n} - SS_C - SS_O$$

$$SS_{GxO} = \frac{1}{il}\sum_j\sum_k T_{.jk.}^2 - \frac{T_{....}^2}{n} - SS_G - SS_O$$

$$SS_{CxGxO} = \frac{1}{l}\sum_i\sum_j\sum_k T_{ijk.}^2 - \frac{T_{....}^2}{n} - SS_C - SS_G - SS_O - SS_{CxG} - SS_{CxO} - SS_{GxO}$$

$$SS_{Error} = SS_{Total} - SS_C - SS_G - SS_O - SS_{CxG} - SS_{CxO} - SS_{GxO} - SS_{CxGxO}$$

The sum of squares are displayed in the table below along with the mean squares (MS) and the F value which is used to determine whether the treatment is significant.

$$MS = \frac{SS}{df}$$

$$F = \frac{MS_{Factor}}{MS_{Error}}$$

Factor	df	SS	MS	F	F_{crit}
Carbon (C)	1	2.98528E+12	2.98528E+12	35.5	4.15
Glass (G)	1	5.35245E+11	5.35245E+11	6.37	4.15
CxG	1	2.33737E+11	2.33737E+11	2.78	4.15
Orientation (O)	1	40574479436	40574479436	0.483	4.15
CxO	1	1.45298E+11	1.45298E+11	1.73	4.15
GxO	1	21869839310	21869839310	0.260	4.15
CxGxO	1	12511642352	12511642352	0.149	4.15
Error	32	2.69038E+12	84074273244		
Total	39	6.66489E+12			

It can be seen from the above results table that the only significant effects are those of the addition of carbon and E-glass fibers.

The following table is for the maximum tensile stress, the significant effects are those of carbon, glass, the carbon and glass interaction, and the glass and orientation interaction.

Factor	df	SS	MS	F	F_{crit}
Carbon (C)	1	283332644.1	283332644.1	53.9	4.15
Glass (G)	1	87272976.4	87272976.4	16.6	4.15
CxG	1	73327224.1	73327224.1	14.0	4.15
Orientation (O)	1	3059196.1	3059196.1	0.582	4.15
CxO	1	15765313.6	15765313.6	3.00	4.15
GxO	1	24258062.5	24258062.5	4.62	4.15
CxGxO	1	11274192.4	11274192.4	2.14	4.15
Error	32	168180158.4	5255629.95		
Total	39	666469767.6			

The following table is the ANOVA for strain at maximum tensile stress. It shows

the carbon, E-glass, and E-glass and orientation interaction have significant effects on the response. The E-glass and orientation interaction effect in the stress and strain ANOVA tables are most likely due to the anisotropy of the Hi Flow mat. In the case of panel 10 chopped E-glass was added to the mat to increase the volume fraction. The other panels contained just the mat with different amounts of carbon and resin. As the carbon and resin amounts vary the glass volume fraction changes but the amount of material stays the same. This changes the significance of the orientation effects of the mat.

Factor	df	SS	MS	F	F_{crit}
Carbon (C)	1	2.51943E-05	2.51943E-05	8.04	4.15
Glass (G)	1	2.11249E-05	2.11249E-05	6.74	4.15
CxG	1	1.24139E-06	1.24139E-06	0.396	4.15
Orientation (O)	1	1.16315E-06	1.16315E-06	0.371	4.15
CxO	1	1.12312E-05	1.12312E-05	3.58	4.15
GxO	1	1.33532E-05	1.33532E-05	4.26	4.15
CxGxO	1	1.29741E-09	1.29741E-09	0.000414	4.15
Error	32	0.000100319	3.13497E-06		
Total	39	0.000173628			

The following table is an ANOVA for flexural modulus. It shows that carbon content is highly significant and dominates the effects on response. This is likely due to the sandwich structure of the composite. The highest portion of the load on a flexed specimen is carried by the bottom surface in tension and the top surface in compression. Therefore with the structure of this composite, when carbon is present it carries the largest of the load which is why it has the highest influence on the response.

Factor	df	SS	MS	F	F_{crit}
Carbon (C)	1	5.23898E+12	5.23898E+12	43.4	4.08
Glass (G)	1	3.21132E+11	3.21132E+11	2.66	4.08
CxG	1	2.34028E+11	2.34028E+11	1.94	4.08
Orientation (O)	1	20263574695	20263574695	0.168	4.08
CxO	1	6902954961	6902954961	0.0572	4.08
GxO	1	22149273913	22149273913	0.184	4.08
CxGxO	1	4.17386E+11	4.17386E+11	3.46	4.08
Error	40	4.8271E+12	1.20677E+11		
Total	47	1.10879E+13			

This next table is an ANOVA of maximum flexural stress. The only factor that has an influence on the response in this case is the carbon percentage. This is likely due to the same reason as described for flexural modulus.

Factor	df	SS	MS	F	F_{crit}
Carbon (C)	1	477938341	477938341	10.7	4.08
Glass (G)	1	128782836	128782836	2.87	4.08
CxG	1	4319400.021	4319400.021	0.0964	4.08
Orientation (O)	1	56882833.52	56882833.52	1.27	4.08
CxO	1	173261000.5	173261000.5	3.87	4.08
GxO	1	1286092.687	1286092.687	0.0287	4.08
CxGxO	1	76046122.69	76046122.69	1.70	4.08
Error	40	1792666295	44816657.37		
Total	47	2711182921			

The last table is the ANOVA for strain at maximum flexural stress. This table determines that none of the factors have a significant effect on the strain response. This is likely due to the large spread of data. The standard deviations for each panel

were large, up to 32% of the strain. Therefore each of the averages were within one standard deviation of each other.

Factor	df	SS	MS	F	F_{crit}
Carbon (C)	1	3.73113E-07	3.73113E-07	0.0282	4.08
Glass (G)	1	1.6413E-06	1.6413E-06	0.124	4.08
CxG	1	1.04394E-05	1.04394E-05	0.790	4.08
Orientation (O)	1	0.000136983	0.000137	10.4	4.08
CxO	1	4.54899E-05	4.54899E-05	3.44	4.08
GxO	1	8.60582E-06	8.60582E-06	0.651	4.08
CxGxO	1	8.21139E-09	8.21139E-09	0.000621	4.08
Error	40	0.000528897	1.32224E-05		
Total	47	0.000732437			

4.3 Synopsis

In this chapter the results were presented in graphical and tabular form. The results were analyzed using analysis of variance and box plots and modeled using the rule of mixtures technique and a simple curve fitting technique. The amount of carbon fiber was found to have the highest significance in contributions to the majority of the material properties. Poisson's ratio was not very sensitive to changes in constituent volume fractions. The orientation effects were difficult to draw conclusions from and were most likely caused by thickness inconsistency throughout the panels. The next chapter will draw conclusions on the research performed for this thesis.

Chapter 5

Conclusions and Future Work

5.1 Conclusions

In this thesis, mechanical properties of advanced chopped fiber reinforced composite structures were determined. The empirical models developed in this thesis for elastic modulus, maximum stresses, and strain at maximum stress provide a design tool for predicting properties of future chopped fiber composites. The industrial partner can use equations 4.1 and 4.2 combined with the confidence interval information collected in this thesis for preliminary design of these novel composite structures.

To produce the data in this thesis, tensile and flexural tests based on ASTM standards for plastics and composite testing were carried out. To manufacture the coupons, a resin transfer molding (RTM) process was used. RTM was chosen because it is an affordable method for manufacturing composite structures. After failure of a small RTM mold, a large mold was designed to create a large flat composite panel. After the panel was molded, it was sent to be waterjet cut using a template of 6 vertical tensile and flexural samples and 9 horizontal tensile and flexural samples.

The experiments were performed using an MTS testing machine and the data was acquired using the load cell, the displacement sensor, and in the case of the tensile tests, a bi-axial extensometer.

The tensile tests were conducted successfully. There was a large data spread, but this is to be expected with chopped fiber composites. Estimates were obtained for tensile modulus, maximum stress, the strain at maximum stress, and Poissons ratio in all three directions. From the data collected, it can be seen that tensile modulus and maximum tensile stress respond very similarly to the amount of carbon or glass fibers added to the composite. Carbon fiber has the most influence on the modulus and stress responses. The tensile strain, on the other hand, does not follow the same trends. The reason for this can be seen from the ANOVA in that the F values for the effect of carbon and E-glass are very close. In the case of maximum stress and tensile modulus the volume fraction of carbon dominates the response. Thus if the carbon volume fraction increases the response will increase essentially independently of the amount of E-glass. With the F values close, if the carbon volume fraction increases and the E-glass volume fraction decreases it may have no effect on the response. It was difficult to conclude on Poisson's ratio. The values of Poisson's ratio were very close between panels. All the averages were within one standard deviation of each other. The tensile modulus and maximum stress response to changes in the constituents were validated and are in agreement with the rule of mixtures.

The flexural tests were also conducted successfully. However, the results found for material properties using the flexure testing methods can not be used for design values. This is due to a flaw in the method of calculating the stresses and strains, and the composites do not fulfill all the basic assumptions of the beam theory used. The flexural modulus, maximum flexural stress, and the strain at maximum flexural stress were estimated using the load and displacement data obtained experimentally. These

material properties are found by graphing the stress verses strain calculated from the load and displacement data. The flexural modulus and stress averages followed the same basic trends as tensile modulus and stress from panel to panel, once again reinforcing the results.

The important results from the flexural testing was the residual strengths experienced with the addition of carbon fiber. This almost plastic behavior of the flexural specimens is a important finding in terms of future impact testing. These findings forecast the excellent impact damage tolerance capabilities of carbon fiber reinforced composite structures. Thus, based on this thesis, more work should be performed on the failure mechanics and determining the levels of residual strength to fully understand this phenomenon.

Each panel had samples cut from it both horizontally and vertically. This was so that any orientation effects would be seen, if existent. With the variability in properties for each sample, it is generally impossible to determine, with certainty, if there is an orientation effect due to the large data scatter. Generally, the means are different in the two orientations, but the for most panels it can not be said the the two orientations are statistically different. The clearest indication of an orientation effect is related to panel 3. This panel has a low spread of test results likely due to the fact that it is just the prefabricated mat and no carbon or E-glass is incorporated in the composite. The mat, though, is stitched it one direction only and this likely is the reason for the dependence on orientation. Other orientation effects that were observed are likely due to thickness inconsistencies in the panel. The horizontal samples were on average thicker than the vertical samples, causing a lower fiber volume fraction and therefore a weaker specimen.

With the inclusion of confidence intervals it is possible to identify more accurate factors of safety for designing composite structures. In order to decide on a factor of

safety there should be no outlying specimens. To accomplish this much work needs to be done on the manufacturing side in order to guarantee consistent samples. An improvement in factor of safety leads to reduced material usage and cost.

5.2 Future Work

The principal focus of the present thesis was to design and implement the experimental capabilities to test hybrid composites in a laboratory setting. Work is currently being undertaken on modeling of resin flow in the RTM process. This will allow for more consistent molding, leading to more reliable confidence intervals so that a lower factor of safety can be used in designing composite structures.

This work will be expanded in the future to include more comprehensive tests. Further testing includes the influence of temperature on the hybrid composite. Also of importance is the response of the advanced composites to fatigue loading. Typically composites have very good fatigue characteristics but it is important to see how the varying carbon and E-glass percentages effects fatigue life. Further down the road, tests on impact of composite structures created using the production method studied in this thesis must be performed.

References

[1] L.S.Sutherland and C.Guedes Soares. The effects of test parameters on the impact response of glass reinforced plastic using an experimental design approach. *Composites Science and Technology*, 63:1–18, 2003.

[2] A. Mills. Automation of carbon fibre preform manufacture for affordable aerospace applications. *Composites Part A: applied science and manufacturing*, 32:955–962, 2001.

[3] R. McIlhagger D. Abraham, S. Matthews. A comparison of physical properties of glass fibre epoxy composites produced by wet lay-up with autoclave consolidation and resin transfer moulding. *Composites Part A: applied science and manufacturing*, 29A:795–801, 1998.

[4] N.S.McDevitt I.P.Datar D.Kim M.G.Jenkins M.Ramulu, P.B.Stickler. Influence of processing methods on the tensile and flexure properties of high temperature composites. *Composites Science and Technology*, 64:1763–1772, 2004.

[5] George Marsh. Composites on the road in the big time. *Reinforced Plastics*, 47(2):33–47, 2003.

[6] V.M. Fonseca S.N.Monteiro J.R.M.d'Almeida C.Z.Paiva Junior, L.H.de Car-

valho. Analysis of the tensile strength of polyester/hybrid ramio-cotton fabric composites. *Polymer Testing*, 23:131–135, 2004.

[7] E.Mader C.Y.Yue X.Hu Y.-W.Mai S.Y.Fu, B.Lauke. Hybrid effects on tensile properties of hybrid short-glass-fiber-and short-carbon-fiber-reinforced polypropylene composites. *Journal of Materials Science*, 36:1243–1251, 2001.

[8] B.Lauke S.Y.Fu. Characterization of tensile behaviour of hybrid short glass fibre/calcite particle/abs composites. *Composites Part A*, 29A:575–583, 1998.

[9] K.Joseph S.Thomas P.Pradeep P.V.Joseph, G.Mathew. Mechanical properties of short sisal fiber-reinforced polypropylene composites: comparison of experimental data with theoretical preditions. *Journal of Applied Polymer Science*, 88:602–611, 2003.

[10] B.C. Mitra-R. Jacobson R. Rowell A.N. Banerjee A.K. Rana, A. Mandal. Short jute fiber-reinforced polypropylene composites: Effect of compatibilzer. *Journal of Applied Polymer Science*, 69:329–338, 1998.

[11] American Society for Testing and Materials. *ASTM D3039 Standard Test Method for Tensile Properties of Polymer Matrix Composite Materials.* ASTM, West Conshohocken, USA, 2000.

[12] American Society for Testing and Materials. *ASTM D638 Standard Test Method for Tensile Properties of Plastic.* ASTM, West Conshohocken, USA, 1999.

[13] American Society for Testing and Materials. *ASTM D790 Standard Test Methods for Flexural Properties of Unreinforced and Reinforced Plastics and Electrical Insulating Materials.* ASTM, West Conshohocken, USA, 1999.

[14] *Composite Materials Handbook.* Department Of Defense, volume 1. polymer matrix composites guidelines for characterization of structural materials edition, 2002.

[15] A.C.Caba A.C. Loos S.D.Moechnig, T.A.Bullions. Mechanical properties of feather fiber glass fiber polypropylene composites. In *ANTEC 2003 Plastics: Annual Technical Conference, Volume 2: Materials*, volume 2, pages 2132–2136. Society of Plastics Engineers, 2003.

[16] C.B.Lee T.M.Wu. Effect of needle density on the mechanical properties of fiber-reinforced polypropylene composites. *Journal of Applied Polymer Science*, 73:2169–2176, 1999.

[17] *Cutting Costs in Short-Run Plastics Injection Molding.* Morgan Industries, Inc., California, USA, 1989.

[18] T.Kincis Yu.M.Tarnopol'skii. *Static test methods for composites.* Van Nostrand Reinhold Company, New York, USA, 1985.

[19] eFunda. Euler beam equation: Kinetics. http://www.efunda.com/formulae/solid mechanics/beams/theory kinematics.cfm, 2004.

[20] D.Bhattacharyya K.Jayaraman. Mechanical performance of woodfibre-waste plastic composite materials. *Science Direct*, 41:307–319, 2004.

[21] K. Friedrich P. Tsotra. Short carbon fiber reinforced epoxy resin/polyaniline blends: Their electrical and mechanical properties. *Science Direct*, 2004.

[22] Davic Bacon. *Design of Experiments for Engineers Workshops.* Council for Continuous Improvement, 1992.

[23] R.A.McLean V.L.Anderson. *Design of Experiments A Realistic Approach.* Marcel Dekker, Inc., New York, USA, 1974.

[24] Charles R. Hicks. *Fundamental Concepts in the Design of Experiments.* Holt, Rinehart and Winston, Inc., New York, USA, 1964.

[25] Peter W.M. John. *Statistical Design and Analysis of Experiments.* The Macmillan Company, New York, USA, 1971.

[26] M.Rajendran M.Muthukumar, D.Mohan. Optimization of mix proportions of mineral aggregates using box behnken design of experiments. *Cement and Concrete Composite*, 25:751 758, 2003.

[27] Jay L. Devore. *Probability and Statistics for Engineering and the Sciences.* Brooks/Cole Publishing Company, California, USA, fourth edition edition, 1995.

[28] Vern Lindberg. Uncertainties and error propagation part i of a manual on uncertainties, graphing, and the vernier caliper. http://www.rit.edu/ uphysics/uncertainties/Uncertaintiespart2.html, July 2000.

[29] Minitab Inc. Minitab statistical software, release 14 for windows. State College, Pennsylvania, 2003.

[30] E.Mader C.Y.Yue X.Hu S.Y.Fu, B.Lauke. Tensile properties of short-glass-fiber- and short-carbon-reinforced polypropylene composites. *Composites Part A: applied science and manufacturing*, 31:1117–1125, 2000.

[31] I.Miskioglu J.P.Konell, J.A.King. Tensile modulus modeling of carbon-filled nylon 6,6 and polycarbonate-based resins. *Journal of Applied Polymer Science*, 90:1716–1728, 2003.

[32] G.N.Karam. Effect of fibre volume on tensile properties of real unidirectional fibre-reinforced composites. *Composites*, 22(2):84–88, 1991.

[33] L.H.Sperling J.A.Manson. *Polymer blends and composites.* Plenum Press, New York, USA, 1976.

[34] H. Smith N.R. Draper. *Applied Regression Analysis.* John Wiley and Sons, Inc., New York, USA, second edition, 1981.

[35] Fred S. Wood Cuthbert Daniel. *Fitting Equations to Data.* John Wiley and Sons, Inc., New York, USA, second edition, 1980.

[36] The MathWorks Inc. Matlab, the laugage of technical computing, release 12.1. 2001.

[37] George Lubin. *Handbook of Composites.* Van Nostrand Reinhold, New York, USA, 1982.

[38] Toray Carbon Fivers America Inc. T700s data sheet.

[39] Reichhold. Atlac itp 31638-00 product bulletin. June 2001.